American journal of physiology – Cell physiology 308.1 (2015): C1-C19

DOI: 10.1152/ajpcell.00272.2014

Title: Depressed excitability and ion currents linked to slow exocytotic fusion pore in chromaffin cells of the SOD1^{G93A} mouse model of amyotrophic lateral sclerosis

Authors: Enrique Calvo-Gallardo[1], Ricardo de Pascual[1,2], José-Carlos Fernández-Morales[1], Juan-Alberto Arranz-Tagarro[1], Marcos Maroto[1], Carmen Nanclares[1], Luis Gandía[1,2], Antonio M. G. de Diego[1], Juan-Fernando Padín[1,2] and Antonio G. García[1,2,3,4]

Affiliations: [1]Instituto Teófilo Hernando, [2]Departamento de Farmacología, Facultad de Medicina, Universidad Autónoma de Madrid, 28029 Madrid, Spain; [3]Servicio de Farmacología Clínica, [4]Instituto de Investigación Sanitaria, Hospital Universitario de La Princesa, 28006 Madrid, Spain.

Running head: Altered fusion pore kinetics in the SOD1^{G93A} mice

Corresponding autor: Antonio G. García, Instituto Teófilo Hernando, Facultad de Medicina, Universidad Autónoma de Madrid, Arzobispo Morcillo, 4. 28029 Madrid, Spain. E-mail: agg@uam.es. Telephone: 0034 914 975 384. Fax: 0034 914 974 630

ABSTRACT

Altered synaptic transmission with excess glutamate release has been implicated in the loss of motoneurons occurring in amyotrophic lateral sclerosis (ALS). Hyperexcitability or hypoexcitability of motoneurons from mice carrying the ALS mutation $SOD1^{G93A}$ (mSOD1) have also been reported. Here we have investigated the excitability, ion currents and the kinetics of the exocytotic fusion pore in chromaffin cells from P90 to P130 days old mSOD1 mice, when motor deficits are already established. With respect to wild type (WT), mSOD1 chromaffin cells had a decrease in the following parameters: 95% in spontaneous action potentials, 70% in nicotinic current for ACh, 35% in Na^+ current, 40% in Ca^{2+}-dependent K^+ current, 53% in voltage-dependent K^+ current. Ca^{2+} current was increased by 37% but the ACh-evoked elevation of cytosolic Ca^{2+} was unchanged. Single exocytotic spike events triggered by ACh had the following differences (mSOD1 versus WT): 36% lower rise rate, 60% higher decay time, 51% higher half-width, 13% lower amplitude, and 61% higher quantal size. The expression of the α3 subtype of nicotinic receptors and proteins of the exocytotic machinery was unchanged in the brain and adrenal medulla of mSOD1, with respect to WT mice. A slower fusion pore opening, expansion, and closure is likely linked to the pronounced reduction in cell excitability and in the ion currents driving action potentials in mSOD1, compared with WT chromaffin cells.

KEYWORDS

Amyotrophic lateral sclerosis
Fusion pore
Chromaffin cells
Exocytosis
Ion channel currents

INTRODUCTION

The selective loss of motoneurons is central-stage in the pathogenesis of amyotrophic lateral sclerosis (ALS). This leads to muscle weakness, atrophy, and spasticity that end up into paralysis, respiratory insufficiency, and patient death in less than 5 years (53). Most ALS cases are sporadic but about 10% of patients have a positive family history; of these, 20% have mutations in the gene for Cu^{2+}/Zn^{2+} superoxide dismutase 1 (SOD1). When modelled in mice, the mutation G93A (glycine to alanine at codon 93) (mSOD1) show adult disease onset from P90 onwards and reproduces the clinical paralytic symptoms of ALS (22, 23), with significant loss of motoneurons (9).

Why motoneurons die in ALS is unknown. The excitotoxic hypothesis implies excess glutamate release in both patients and transgenic mice (6, 31, 52, 56, 60). This will lead to altered Ca^{2+} homeostasis, excess production of free radicals, and apoptotic death of motoneurons (18, 44, 62). Consistent with this is the fact that riluzole, the only medicine so far approved to treat ALS (2, 53), inhibits the exocytotic release of glutamate (38). Also, it has been reported that cerebrospinal fluid of ALS patients augments the basal concentration of cytosolic calcium ($[Ca^{2+}]_c$) and elicits motoneuron death (65).

The excitotoxic hypothesis implies that a chronically hyperexcitable motoneuron would fire more action potentials (APs) and consequently more Ca^{2+} will enter into its cytoplasm, eventually eliciting its death (27, 33, 62). Some reports suggest that embryo motoneurons and cortical neurons of mSOD1 mice are hyperexcitable (33, 48, 50). However, other reports show normal excitability at neonatal age (51) or even hypoexcitability at adult P30-P80 mSOD1 mice (14).

We here propose the hypothesis that a more general alteration in the fine tuning of neuronal excitability and the exocytotic machinery may underlie the pathogenic features of ALS, and that these alterations could also be present in adrenal chromaffin cells. In fact, altered exocytosis in chromaffin cells have

been shown in the APP/PS1 mouse model of Alzheimer's disease (AD) (13), in the knock-out mouse model of the huntingtin-associated protein 1 (HAP1), a model of Huntington's disease (HD) (35), and in mice carrying specific mutations in proteins of the exocytotic machine (55, 59). We have studied here the cell excitability, ion currents, Ca^{2+} signals, and the quantal release of catecholamine in chromaffin cells from wild type (WT) and mSOD1 mice. We have found a pronounced depression of cell excitability and ion currents associated to a slow kinetics of the fusion pore with higher quantal size, in mSOD1 compared with WT chromaffin cells.

MATERIALS AND METHODS

Animals

Experiments were conducted according to the recommendation of the Ethics Committee from Universidad Autónoma de Madrid on the use of animals for laboratory experimentation, in accordance with the code of ethics and guidelines established by European Community Directive (2010/63/EU) and Spanish legislation (RD53/2013). All efforts were made to avoid animal suffering and to use the minimum number of animals allowed by the experimental protocol and the statistical power of group data. Mice were housed individually under controlled temperature and lighting conditions with food and water provided *ad libitum* and housed on a 12:12 h light cycle.

Male *B6.Cg-Tg(SOD1-G93A)1Gur/J* mice, hereafter referred to as mSOD1, were purchased from The Jackson Laboratory, Bar Harbor, Maine (stock #004435). These mice over-express a point mutated form of the human SOD1 gene (single amino acid substitution of glycine to alanine at codon 93) driven by the endogenous human promoter. Offspring hemizygous for the mutant SOD1 transgene used in this study were produced by strict crossings of hemizygous male $SOD1^{G93A}$ mice with wild-type C57BL/6J inbred females to maintain the mutant transgene on a C57BL/6 congenic background. We trust "The Jackson Laboratory's Genotype Promise" that ensures the right genotyping of the animals. The same number of C57BL/6J wild type mice, hereafter referred to as WT, were used as controls. Mice were used at postnatal days P90 to P130 and henceforth will be referred to as P100; at this age the animals show adult disease onset (22, 23) and significant loss of vulnerable spinal motoneurons (9).

Primary culture of mouse chromaffin cells

Mice were sacrificed by cervical dislocation. Both adrenal glands from a mouse were rapidly collected and placed in ice-cold Locke's solution of the

following composition (in mM): 154 NaCl, 5.5 KCl, 3.6 $NaHCO_3$, 10 HEPES and 5.5 D-glucose (pH 7.4, NaOH). Glands were fat-trimmed and medullae were isolated by removing the cortex. Then the medullae were placed in a tube containing 200 µL Locke's solution with papain (25 U/ml) for tissue digestion during 30 min. This solution was exchanged by 1 ml DMEM, repeating the exchange 3 times and leaving finally 120 µl of DMEM. Then medullae were minced first with a 1 ml micropipette and then with a 200 µl micropipette. Finally, the residual medulla fragments were discarded and 10-20 µl drops of cell-containing solution from the minced extracts were plated on poly-D-lysine-coated coverslips of one or two 12-well plates. After 30 min in an incubator (37 °C, water-saturated and 5% CO_2 atmosphere) 1 ml DMEM supplemented with 5% fetal bovine serum, 50 IU/ml penicillin, and 50 µg/ml streptomycin were added to each well and remained in the incubator for 1 to 2 days during which experiments were done.

Monitoring of cell excitability and ion currents

Recordings of membrane potential (V_m) and APs were made under the current-clamp mode in the whole-cell configuration of the patch-clamp technique (24), which allows the observation of spontaneous variations in the V_m. Cells were superfused with control Tyrode solution at pH 7.4 containing (in mM): 137 NaCl, 1 $MgCl_2$, 2 $CaCl_2$ and 10 HEPES/NaOH; an intracellular solution at pH 7.4 containing (in mM) 135 KCl, 10 NaCl, 10 HEPES, 1 $MgCl_2$ and 5 EGTA was introduced in the patch-clamp pipette.

Inward currents through nicotinic receptor ion channels (I_{ACh}), voltage-activated sodium channels (I_{Na}), voltage-activated calcium channels (I_{Ca}), voltage-activated potassium channels ($I_{K(V)}$) and calcium-dependent potassium channels ($I_{K(Ca)}$) were recorded using the voltage-clamp mode of the whole-cell configuration of the patch-clamp technique (24). Whole-cell recordings were made with fire-polished borosilicate pipettes (resistance 2-5 MΩ) that were mounted on the headstage of an EPC-9 patch-clamp amplifier (HEKA Electronic, Lambrecht, Germany), allowing cancellation of capacitative

transients and compensation of series resistance. Data were acquired with a sample frequency of 20 kHz by using PULSE 8.74 software (HEKA Elektronik). The data analysis was performed with Igor Pro (Wavemetrics, Lake Oswego, OR, USA) and PULSE programs (HEKA Elektronik). Coverslips containing the cells were placed on an experimental chamber mounted on the stage of a Nikon Diaphot inverted microscope. Cells were continuously superfused with a control Tyrode solution at pH 7.4 containing (in mM): 137 NaCl, 1 $MgCl_2$, 2 $CaCl_2$ and 10 HEPES/NaOH. Once the patch membrane was ruptured and the whole-cell configuration of the patch-clamp technique had been established, the cell was locally, rapidly and constantly superfused with an extracellular solution of similar composition to the chamber solution, but containing nominally 0 mM Ca^{2+} to measure I_{Na}, and 2 mM Ca^{2+} to measure I_{ACh}, I_{Ca} and I_K.

Cells were internally dialysed with an intracellular solution containing (in mM): 100 CsCl, 14 EGTA, 20 TEA-Cl, 10 NaCl, 5 Mg-ATP, 0.3 Na-GTP, and 20 HEPES/CsOH (pH 7.3) for the recording of I_{Na}, I_{Ca} and I_{ACh}; for recording I_K the intracellular solution had the following composition (in mM): 135 KCl, 14 EGTA, 10 NaCl, 5 Mg-ATP, 0.3 Na-GTP, and 20 HEPES/KOH (pH 7.3). The external solutions were rapidly exchanged using electronically driven miniature solenoid valves coupled to a multi-barrel concentration clamp device, the common outlet of which was placed within 100 µm of the cell to be patched. The flow rate was 1 ml/min and was regulated by gravity.

For measuring the different currents, cells were held at −80 mV; I_{Na} was generated by 10 ms depolarising pulses to −10 mV, I_{Ca} was generated by 50 ms depolarising pulses to −10 or 0 mV; I_{ACh} was generated by the application of 250 ms ACh pulses (100 µM), and I_K was generated by the application of a 10 ms pre-depolarising command to +30 mV followed by a 400 ms full depolarisation pulse to +120 mV. All experiments were performed at room temperature (24 ± 2 °C) on cells from 1 to 2 days after culture.

Measurements of changes in the cytosolic calcium concentration

Chromaffin cells were incubated for 1 h at 37 °C in DMEM medium containing the calcium probe fura-2 acetoxymethyl ester (fura-2AM; 10 μM). After this incubation period, the coverslips were mounted in a chamber and cells were washed and covered with Tyrode solution. The setup for fluorescence recordings was composed of a Leica DMI 4000 B inverted light microscope (Leica Microsystems; Barcelona, Spain) equipped with an oil immersion objective (Leica 40× Plan Apo; numerical aperture 1.25). Once the cells were placed on the microscope, they were continuously superfused by means of a five-way superfusion system at 1 ml/min with a common outlet 0.28 mm-tube driven by electrically controlled valves with Tyrode solution. Fura-2AM was excited alternatively at 340 ± 10 and 387 ± 10 nm using a Küber CODIX xenon arc lamp (Leica). Emitted fluorescence was collected through a 540 ± 20 nm emission filter and measured with an intensified charge coupled device camera (Hamamatsu camera controller C10600 orca R^2; Japan). Fluorescence images were generated at 1-s intervals. All experiments were performed at room temperature (24 ± 2 °C) on cells from 1 to 2 days after culture.

Amperometric recordings

Quantal release of catecholamine was measured with amperometry (10, 64). Electrodes were built as previously described (30) by introducing a 10 μm diameter graphite fibre (Amoco, now part of BP-Group, London, UK) into glass capillary tubes (Kimble-Kontes, Vineland, NJ, USA). These tubes were then pulled (Narishige PC-10 pipette puller, Narishige, Tokyo, Japan), and the carbon fibre was inserted in both thin ends of the pulled tube and was cut with a pair of small scissors obtaining thus two pipettes with a carbon fibre piece sticking out of each tip. The tip was sealed by a two-component epoxy (EPIKOTE 828-Miller-Stephenson, Danbury, CT, USA); and *m*-phenylendiamine, 14% (Aldrich, Steimheim, Germany). The electrodes were left overnight to dry, introduced into an oven at 100 °C for 2 h, and then kept another 2 h at 150 °C. The amperometer was homemade (UAM workshop, Madrid, Spain) and connected to an interface (PowerLab/4SP, ADInstruments, Oxford, UK) that digitised the signal at 10 kHz sending it to a personal computer

that displayed it within the Pulse v8.74 software (HEKA Elektronik). A 700-mV potential was applied to the electrode with respect to an AgCl ground electrode. The electrodes were calibrated following good amperometric practices (36) by perfusing 50 µM norepinephrine dissolved in standard Tyrode and measuring the current elicited; only electrodes that yielded a current between 200 and 400 pA were used. The coverslips were mounted in a chamber on a Nikon Diaphot inverted microscope used to localise the target cell, which was continuously superfused by means of a five-way superfusion system with a common outlet driven by electrically controlled valves, with a Tyrode solution composed of (in mM) 137 NaCl, 1 $MgCl_2$, 5 KCl, 2 $CaCl_2$, 10 HEPES and 10 glucose (pH 7.4, NaOH). The high K^+ solutions were prepared by replacing equiosmolar concentrations of NaCl with KCl. At the time of experiment performance, proper amounts of drug stock solutions were freshly dissolved into the Tyrode solution. All experiments were performed at room temperature (24 ± 2 °C) on cells from 1 to 2 days after culture.

Immunoblotting and image analysis of the expression of proteins of the exocytotic machinery and the α3 subunit of nicotinic receptors

Motor cortex, hippocampus, spinal cord and adrenal glands were removed from the mice, and membrane proteins were extracted using the MEM-PER™ Membrane Protein Extraction Kit (Thermo Scientific, Rockford, IL, USA) following the manufacturer´s instructions. At all times, proteins were in the presence of protease inhibitors (Halt™ Protease Inhibitor Cocktail; Thermo Scientific). Proteins were quantified using the Bicinchoninic Acid Protein Assay (G-Biosciences, St. Louis, MO, USA). Proteins (20 µg) were resolved by SDS-PAGE (12%) and transferred to Immobilon-P® Transfer Membrane (Millipore Corporation, Billerica, MA, USA). Membranes were blocked in Tris-buffered saline with 0.05% Tween® 20 containing 4% bovine serum albumin, and incubated for 2 h at room temperature with primary antibodies anti-synaptotagmin 1 (SYT1, 1:200), anti-synaptotagmin 7 (SYT7, 1:200), anti-syntaxin 1 (STX1, 1:200), anti-synaptosomal-associated protein 25 (SNP25, 1:200), anti-vesicle-associated membrane protein 2 (VAMP2, 1:200) and anti-

neuronal ACh receptor subunit α3 (NACHRA3, 1:200), all of them from Santa Cruz Biotechnology (Dallas, TX, USA), and with anti-β-actin (1:100.000; Sigma-Aldrich, St. Louis, MO, USA) as loading control; then, for 45 min with secondary antibodies conjugated with peroxidase (1:10.000; Santa Cruz Biotechnology). The membrane was developed using the ECL Select^{TM} Western Blotting Detection Reagent (GE Healthcare, Chalfont St. Giles, UK). Different band intensities corresponding to immunoblot detection of protein samples were quantified using Scion Image® Alpha 4.0.3.2 programme (Scion Corporation, USA).

Rota-Rod test

The Rota-Rod apparatus (Stoelting Co., Wood Dale, IL, USA) was used to assess motor performance. Mice were challenged with an initial speed of 8 rpm and an increase of 1 rpm each 8 seconds until they fell down. The time spent walking on the Rota-Rod was measured and time from 10 repetitions was averaged; 180 seconds was chosen as the arbitrary cut-off time. Mice were trained for 1 day (training day, Trd) to get acquainted with the Rota-Rod apparatus for the test day (Td) in consecutive days. Different mice at P90 and P130 ages were used.

Statistical analysis

Ion currents and cell excitability data analysis were performed using the GraphPad Prism version 5.01 for Windows (GraphPad Prism Software, San Diego, CA, USA). Student's t-test or one-way ANOVA followed by Tukey or Dunnett post hoc tests were used to determine statistical significance between means. *$P < 0.05$ was taken as the limit of significance; ** and *** show a statistical significance of $P < 0.01$ and $P < 0.001$, respectively.

Data from measurement of changes in the $[Ca^{2+}]_c$ was obtained from LAS AF software and Ascent software version 2.4.2. Graphs and the mathematical analyses were performed using the GraphPad Prism software,

version 5.01 (GraphPad Software Inc.). Areas were calculated by integrating the $[Ca^{2+}]_c$ transient over time during the stimulus duration by means of Origin Pro 8 SR2 software, version 8.0891 (OriginLab Corporation, Northampton, MA, USA). Areas were worked out by the integration of the input data set by using the trapezoidal rule. Results shown in the text and figures are expressed as mean ± SEM Statistical analyses were carried out with one-way ANOVA test and Tukey post-hoc analyses. *P < 0.05 was taken as the limit of significance; ** and *** show a statistical significance of P < 0.01 and P < 0.001, respectively.

Amperometry data analysis was carried out on a personal computer using Excel software (Microsoft, Redmond, WA, USA) and IgorPro software (Wavemetrics). Total amperometric quantal charge was calculated by integrating the amperometric current over time during the stimulus duration with a homemade macro written in IgorPro software. The number of spikes greater than 5 pA was manually counted on an extended graph displayed in the computer screen. A ruler was drawn at 5 pA and only the spikes going above the threshold amplitude were considered. The kinetic analysis of single amperometric events (spikes) was performed as previously described (21) using a macro written in IgorPro software (41). Median values for all the spikes of each cell were obtained and then pooled together for statistical comparison; this method helps overcoming the large variability in spike number and spike kinetics by giving each cell the same weight independently of the number of spikes produced. Differences between means of group data fitting a normal distribution were assessed by using either analysis of variance or Kruskal-Wallis test for comparison among multiple groups or Student's *t* test for comparison between two groups. *P < 0.05 was taken as the limit of significance; ** and *** show a statistical significance of P < 0.01 and P < 0.001, respectively.

Comparisons between groups from immunoblotting and image analysis of the expression of proteins, were performed by one-way analysis of variance (ANOVA) followed by the Newman-Keuls post hoc test or by the unpaired Student's t-test using the Graph Pad Prism software version 5.01. $*^{/\#}P$ < 0.05

was taken as the limit of significance. ** and *** show a statistical significance of $P < 0.01$ and $P < 0.001$, respectively.

Data from Rota-Rod test are means from 10 repetitions of Trd and Td of different mice at P90 and P130 ages. *$P < 0.05$ was taken as the limit of significance; ** and *** show a statistical significance of $P < 0.01$ and $P < 0.001$, respectively.

Materials and chemicals

The calcium binding probe fura-2AM was purchased from Invitrogen (Eugene, OR, USA). Acetylcholine chloride and all other chemical components used in this study for cell cultures and the various experiments were obtained from Sigma-Aldrich and GIBCO-Invitrogen (Barcelona, Spain).

RESULTS

To discern about possible differences in the stimulus-secretion coupling process been WT and mSOD1 chromaffin cells, we explored the various steps in the chain of events involved in such process. Those steps include chromaffin cell excitability and the firing of spontaneous APs, ion currents, $[Ca^{2+}]_c$ transients, and the exocytotic release of catecholamine, including the kinetic analysis of the single-vesicle amperometric spike. With the thorough analysis of those events we expected to raise a hypothesis to explain the changes in the quantal release of catecholamines. Furthermore, although ACh and high-K^+ quantitatively elicit similar Ca^{2+}-dependent catecholamine release responses (17) we later on showed that the Ca^{2+} transients and the secretory responses elicited by ACh and K^+ considerably differed (8). Thus we analysed here the $[Ca^{2+}]_c$ transients and the kinetics of the quantal release of catecholamine in chromaffin cells from WT and mSOD1 mice stimulated with ACh or high-K^+.

Excitability of chromaffin cells from WT and mSOD1 mice

To determine the resting V_m, cells were sealed under the voltage-clamp mode and held at a potential of −80 mV until series resistance was lower than 20 MΩ. Then the amplifier was switched to current-clamp mode and current injection set to 0 pA. In 15 cells from 6 different WT mice, V_m was −67.8 ± 2.05 mV and in 31 cells from 7 different mSOD1, V_m was −62.85 ± 1.9 mV (Figure 1D). These values agree with those found in chromaffin cells from various animal species that ranged between −50 and −80 mV (reviewed in 12).

In spite of the fact they had similar V_m, the firing of spontaneous APs considerably differed in chromaffin cells of WT and mSOD1 mice. For instance, the example WT cell of Figure 1A had a V_m of around −60 mV and initially fired a burst of high-rate APs during the first 70 s; thereafter, the cell had silent periods with a few scattered APs. Figure 1B corresponds to an example mSOD1 cell with only a few APs scattered along the 5-min recording period. In 15 WT cells from 6 different mice, we counted 57.6 ± 12 APs during the 5 min

recording period; in sharp contrast, in the 31 mSOD1 cells from 7 mice we only counted 2.6 ± 1 APs (Figure 1C).

Whole-cell ion currents of chromaffin cells from WT and mSOD1 mice

Whole-cell ion currents were recorded in WT and mSOD1 chromaffin cells voltage-clamped at −80 mV. I_{ACh} were elicited by the application of a 250 ms pulse of an extracellular solution containing 100 µM ACh. ACh pulses were applied at regular 2 min intervals. Figure 2A shows the I_{ACh} traces generated by the application of 5 sequential pulses of ACh to an example WT cell. Figure 2B shows 5 I_{ACh} traces obtained on an example mSOD1 cell showing a smaller peak amplitude. Two example I_{ACh} obtained from a WT and a mSOD1 cell are displayed in Figure 2C; in both cases, current inactivation is likely due to the well known desensitisation of nicotinic receptors upon their exposure to ACh (29, 46). In 13 cells from 4 WT mice, I_{ACh} peak was 3.87 ± 0.32 nA while in 43 cells from 9 mSOD1 mice was 1.16 ± 0.06 nA, a 70% diminution (Figure 2D).

I_K were investigated using a two-step depolarising pulse protocol. First, a 10 ms pre-depolarising command to +30 mV was given in order to allow Ca^{2+} entry and the activation of the calcium-dependent component of I_K; then, a 400 ms depolarising pulse to +120 mV was applied to recruit both the Ca^{2+}-dependent and the voltage dependent components of I_K (see protocol on top of Figure 2E). The I_K traces of Figure 2E were taken from a WT and mSOD1 cell subjected to the two-step depolarising pulse protocol. Initially there is a large outward current component that inactivates in about 100 ms to a sustained plateau; these two components are due, respectively, to activation of $I_{K(Ca)}$ and activation of $I_{K(V)}$. $I_{K(Ca)}$ is activated by the $[Ca^{2+}]_c$ transient generated by the pre-pulse and inactivates upon clearance of such transient to give rise to the sustained plateau, that is due to voltage-dependent K^+ channels, which remain open for the entire 400 ms depolarising pulse (45). Figure 2E shows that $I_{K(Ca)}$ and $I_{K(V)}$ components of I_K were present in mSOD1 cells; they however were substantially lower than those recorded in the WT cell. These differences are better illustrated in the bar diagram of Figure 2F. Thus, the averaged $I_{K(Ca)}$

component of 30 cells from 5 WT mice was 6.25 ± 0.46 nA compared with 3.75 ± 0.47 nA in 8 cells from mSOD1 mice, a 40% diminution; the values for the $I_{K(V)}$ component were 2.4 ± 0.13 nA and 1.12 ± 0.22 nA, for WT and mSOD1 cells, respectively (a 53% diminution).

I_{Ca} were generated by application of 50 ms test depolarising pulses to 0 mV, as shown in the protocol on top of Figure 3A; in this panel, two superimposed current traces from example WT and mSOD1 cells, with their initial rapidly inactivating I_{Na} and later slow-inactivating I_{Ca}, are shown. Averaged peak amplitude of I_{Ca} for WT and mSOD1 cells is shown in Figure 3B, with 170 ± 21.6 pA for WT cells and 270 ± 28.1 pA for mSOD1 cells, a 37% increase. No differences of current kinetics between both cell types were observed.

Finally, I_{Na} were generated with test depolarising pulses to −10 mV, given at 10 s intervals. I_{Na} traces obtained in WT and mSOD1 cells are shown in Figure 3C; peak I_{Na} amplitude was 20% smaller in the latter, respect to the former. Pooled data from 49 cells of 6 WT mice gave an I_{Na} peak amplitude of 1.41 ± 0.12 nA, while in 25 cells from 6 mSOD1 mice I_{Na} averaged 0.92 ± 0.08 nA, a 35% decrease (Figure 3D).

Cytosolic calcium transients generated by cell depolarisation with acetylcholine or high-potassium in chromaffin cells from WT and mSOD1 mice

It is well established that ACh and high K^+ cause cell depolarisation, enhanced Ca^{2+} entry through voltage-activated calcium channels (VACCs), elevation of $[Ca^{2+}]_c$, and the activation of the exocytotic release of catecholamine from chromaffin cells (1, 12, 15, 43). From a quantitative point of view, ACh and high K^+ trigger similar catecholamine release responses; however, the $[Ca^{2+}]_c$ transients generated by these two secretagogues are quite different (8). Therefore, we next explored the $[Ca^{2+}]_c$ transients generated by ACh and high K^+ in fura-2AM loaded WT and mSOD1 chromaffin cells. After an initial 3 min period to get a stable resting baseline, cells were challenged with Tyrode solutions containing supramaximal depolarising ACh concentrations

(100 μM) or high K^+ (75 mM) during 1 min. This protocol was similar to that used to monitor the quantal release of catecholamine (see later). A given cell was stimulated with ACh or K^+ only once.

Example records of the time course of the $[Ca^{2+}]_c$ elevations produced by ACh and K^+ in WT and mSOD1 chromaffin cells are shown in Figure 4A and 4B, respectively. Although the ACh-evoked $[Ca^{2+}]_c$ transients were similar in WT and mSOD1 cells, the K^+-evoked $[Ca^{2+}]_c$ transients were notably higher in mSOD1 cells, with respect to WT cells. This is better illustrated in the bar graphs of Figure 4C,D and E, showing that in WT and mSOD1 cells challenged with ACh time to peak (t_{max}), peak amplitude, and area are similar for both types of cells. This was not the case for K^+; in mSOD1 cells t_{max} is 20% lower with respect to WT cells. However, peak amplitude and area are 88 and 100% higher, respectively. Thus, the K^+-elicited $[Ca^{2+}]_c$ transient had a faster activation as well as almost 2-fold enhanced $[Ca^{2+}]_c$ in mSOD1 with respect to WT cells. This agrees with the higher I_{Ca} current observed in mSOD1 cells with respect to WT cells (Figure 3B).

Quantal catecholamine release responses triggered by acetylcholine or high potassium in chromaffin cells from WT and mSOD1 mice

To study the quantal release of catecholamine, all experiments began with an initial 5 min perifusion resting period with a standard Tyrode solution for adaptation of the targeted cell to its environment. None or few spontaneous amperometric secretory spikes were usually seen during this period. To stimulate exocytosis, the basal Tyrode solution containing 2 mM Ca^{2+} was quickly switched to another containing 100 μM ACh or 75 mM K^+ that bathed the cell for 1 min. This long stimulation period was used for two reasons: (1) we sought to get the maximal number of spikes to augment the power of statistical analysis of single exocytotic events; and (2) we also wished to explore potential differences in the time course of secretion linked to vesicle pool exhaustion and/or to the inactivation of VACCs (25, 61). A given cell from a culture dish

449 was stimulated with ACh only once. About 75% of the tested mSOD1 cells and
450 85% of the WT cells responded to ACh.
451
452 Figure 5A shows the spike burst produced by ACh in an example control
453 cell; baseline was stable during the burst indicating the absence of overlapping
454 spikes. Figure 5B shows a spike record from an example mSOD1 cell. Once
455 more, in this cell no baseline elevation was produced although an initial high-
456 frequency spike burst occurred; this was followed by a period with few spikes.
457 Pooled data on cumulative secretion versus time calculated at 5 s intervals from
458 experiments similar to those shown in the example records of Figure 5A,B were
459 plotted in Figure 5C. In both cell types an initial faster rate of secretion during
460 the first 10 s of the ACh pulse was followed by slower secretion rates that were
461 slowly increasing along the next 50 s period. In mSOD1 cells the initial secretion
462 rate was 21.7% slower (time constant for activation, τ_a = 13.72 s) as compared
463 with WT cells (τ_a = 11.27 s). The integrated secretion (area in pC of all spikes
464 secreted by each ACh pulse) is plotted in Figure 5D; this total secretion was
465 46.6% higher in mSOD1 cells. However, in spite of this difference, the number
466 of spikes per ACh stimulus was similar, 24.55 ± 2.22 for WT cells and 21.06 ±
467 1.22 for mSOD1 cells (Figure 5E). The quantal size (single-vesicle content of
468 catecholamine, *Q*) was 1.6-fold higher in mSOD1 cells (0.47 ± 0.03 pC) with
469 respect to WT cells (0.31 ± 0.02 pC) (Figure 5F and Table 1). Thus, this higher
470 total secretion with similar spike numbers could be explained by this greater
471 quantal size of mSOD1 with respect to WT cells.
472
473 Concerning K^+ stimulation (75 mM, 1 min), most WT and mSOD1 (>95%)
474 responded to this stimulus. The example WT cells displayed in Figure 6A,B
475 generated an initial spike burst followed by more infrequent spikes, indicating a
476 slower rate of secretion at later stages of the K^+ stimulation period. Of note was
477 baseline elevation at the beginning of the K^+ pulse, suggesting the presence of
478 overlapping spikes due to fast almost simultaneous exocytosis of docked
479 vesicles of a readily releasable vesicle pool (RRP) (21, 40, 43). Cumulative
480 secretion versus time measured at 5 s intervals was plotted in Figure 6C. Unlike
481 for ACh, the initial secretion was similar in WT cells (τ_a = 10.71 s) and mSOD1

cells (τ_a = 10.75 s). The two curves run in parallel and exhibited a low rate of increasing secretion. The integrated secretion (area in pC of all spikes secreted per each K^+ pulse) is plotted in Figure 6D; this secretion was similar in both cell types, around 12-13 pC. The total spike number (20.44 ± 1.98 for WT and 23.8 ± 1.76 for mSOD1) (Figure 6E) and the *Q* (0.4 ± 0.02 pC for WT and 0.42 ± 0.03 pC for mSOD1) were also similar (Figure 6F and Table 1).

Spike frequency histograms counted at 2 s intervals during the 60 s stimulation periods with ACh or K^+, are shown in Figure 7A-D. The decay of the rate of spike frequency was best fitted to a single exponential in WT and mSOD1 cells. With ACh stimulation the time constant for inactivation (τ_i) of spike frequency was 8.1 s and 8.23 s, respectively, for WT and mSOD1 cells; in the case of K^+, τ_i amounted to 4.43 s and 5.36 s for WT and mSOD1 cells, respectively (Figure 7E). Thus, the inactivation rate was 15% and 12% slower in mSOD1 cells, respectively for ACh or K^+. Of note was the fact that spike frequency with ACh had a smaller plateau in mSOD1 cells (0.77%) than in control cells (1.26%) (Figure 7A,B). These differences were not apparent with K^+ (1.02% versus 1.17%, for WT and mSOD1 cells, respectively) (Figure 7C,D).

Types of secretory spike events in chromaffin cells from WT and mSOD1 mice

We next counted and analysed the different types of spike events present in secretory traces generated by 1-min stimulation with ACh or K^+. Figure 9 shows examples of the different subtypes of spikes analysed, and Table 2 contains pooled results on the relative percentage of the different subtypes of spikes analysed. With ACh stimulation, spikes with foot were 59.56% and 65.71% for WT and mSOD1 cells, respectively. With K^+, the number of spikes with foot was similar in both cell types, around 70% (no statistically significant difference). Although an increase of spikes with foot seemed apparent in mSOD1 cells (65.71% with ACh and 73.1% with K^+), these differences were only statistically significant with ACh compared with the values of WT cells (59.56% with ACh and 67.94% with K^+). We also compared values

514 of ACh and K^+ stimuli and differences were statistically significant both in WT
515 and mSOD1 cells (Table 2).
516
517 Multiple spike events (overlapping spikes) indicate near-simultaneous
518 quantal catecholamine release from vesicles belonging to a RRP. For instance,
519 in a previous study we found as much as 30% overlapping spikes in cells from
520 spontaneously hypertensive rats (SHRs) that likely had a larger RRP and hence
521 they responded with massive exocytotic events upon their stimulation with ACh
522 or K^+; in contrast, cells from normotensive rats had only 15% of overlapping
523 spikes (40). Compared with the rat, cells from control mice had only 3.91% of
524 multiple spike events when stimulated with ACh and around 5.69% when
525 stimulated with K^+ (Figure 9B,C, Table 2). Similar values were obtained in cells
526 from mSOD1 (4.15% and 5.09%, respectively) (Figure 9E,F, Table 2). Flickers
527 are defined as small amounts of catecholamine release through a narrow fusion
528 pore that opens transiently. Examples of these flickers are shown in Figure
529 9B,C (WT cells stimulated respectively with ACh or K^+) and in Figure 9E,F
530 (mSOD1 cells stimulated respectively with ACh or K^+). We found that 69.8% of
531 ACh-elicited secretory responses from control cells had at least 1 flicker; this
532 was higher than the value of 60.3% obtained when these cells were stimulated
533 with K^+. Of those, 6.9% and 7.52% of the total spike number were flickers. On
534 the other hand, 69.6% and 82.4% of mSOD1 cells stimulated with ACh and K^+
535 had 1 flicker at least, and flickers were 8.84% and 8.13% of the total spike
536 number, respectively (Table 2).
537
538 *Kinetic analysis of single exocytotic events occurring in the secretory responses*
539 *triggered by acetylcholine and high potassium in chromaffin cells from WT and*
540 *mSOD1 mice*
541
542 Figure 8A shows a schematic model of an amperometric secretory spike
543 with foot, indicating the parameters that we measured according to the criteria
544 established by Machado *et al.* (36) for good practices in single-cell
545 amperometry. Four types of comparative analyses were performed: (i) WT
546 (2034 spikes, 63 cells) versus mSOD1 cells (1357 spikes from 69 cells)

547 stimulated with ACh; (ii) WT (1848 spikes, 58 cells) versus mSOD1 cells (1761
548 spikes, 74 cells) stimulated with K^+; (iii) WT cells stimulated with ACh versus K^+
549 and (iv) mSOD1 cells stimulated with ACh versus K^+.
550
551 (i) All parameters studied on WT and mSOD1 cells indirectly
552 depolarised with the physiological neurotransmitter ACh, exhibited statistically
553 significant differences (Table 1). Thus, compared with WT, mSOD1 cells had
554 the following changes: 35.94% lower rise rate, 60.7% longer decay time, 55.3%
555 higher half-amplitude time (half-width, $t_{1/2}$), 16.62% lower amplitude (I_{max}), and
556 52.24% higher *Q*. Averaged spikes with these parameters resulted in a
557 narrower but faster spike for WT cells, compared with a slower spike with higher
558 *Q* for mSOD1; this indicated a slower but higher exocytotic release of
559 catecholamine per single vesicle in the latter, compared with the former as
560 indicated in the averaged overlapping spikes of Figure 8B.
561
562 (ii) Surprisingly, all kinetic parameters of spikes recorded from WT
563 and mSOD1 cells directly depolarised with K^+ had similar values (Table 1). This
564 indicated that the averaged exocytotic spike did not differ between both cell
565 types when they were directly depolarised with K^+, as the overlapping averaged
566 spikes indicate in Figure 8C.
567
568 (iii) We also noted some kinetic differences in the spikes generated by
569 ACh or K^+ stimulation of WT cells. Thus, compared with ACh stimulated cells
570 (indirect depolarisation through intermittent APs), the K^+ stimulated cells
571 (continuous direct depolarisation) had 27.62% lower rise rate, 27.05% higher
572 decay time, 21.57% higher $t_{1/2}$, 12.97% lower I_{max} and 28.77% higher *Q*. The
573 overlapping averaged spikes of Figure 8D indicates a faster but smaller release
574 of catecholamine when WT cells were stimulated with ACh, compared with K^+.
575
576 (iv) Finally, we compared the kinetic parameters of the secretory
577 events recorded in mSOD1 cells stimulated with ACh or K^+, which showed only
578 minor differences. For instance, compared with ACh, the K^+ elicited spikes had
579 30.24% higher rise rate, 16.43% lower decay time and 17.81% lower $t_{1/2}$; the

rest of the parameters were similar (no statistically significant differences). Overlapping averaged spikes indicated that the K^+ elicited secretory response was slightly faster but with *Q* similar to ACh (Figure 8E).

Spikes with foot were slightly more frequent (10.33%) in ACh stimulated mSOD1 cells, compared with WT cells (Table 3). Foot duration was 30.8% longer and had 22.95% lower amplitude in mSOD1 cells compared with WT cells. No statistically significant differences were observed between both cell types upon their stimulation with K^+ (Table 3).

Immunoblot analysis of the expression of proteins of the exocytotic machinery and the α3 subunit of nicotinic receptors in WT and mSOD1 mice.

The detailed analysis of the kinetics of amperometric secretory spikes is contributing to a better understanding of the molecular mechanisms through which the different proteic components of the exocytotic machinery regulate the last steps of exocytosis and hence, of neurotransmitter release. In fact, chromaffin cells from transgenic mice with genetic manipulations of SNARE proteins have extensively been used to explore specific mutations of those proteins on the formation and expansion of the fusion pore (58). We therefore thought of interest to explore the expression of three SNARE proteins and synaptotagmin in the adrenal medulla, the brain cortex and hippocampus, as well as the spinal cord of WT and mSOD1 mice.

Figure 10 displays the relative densities of SYT7 (A), STX1 (B), SNP25 (C) and VAMP2 (D) in the adrenal medulla of WT and mSOD1 mice. We found no statistical differences in the relative expression level of SYT7, STX1, SNP25 and VAMP2 in the adrenal medulla between WT and mSOD1; a decreased 20% expression of VAMP2 was at the limit of statistical significance. We also monitored the expression of the NACHRA3 known to be expressed at high density in chromaffin cells and to mediate the catecholamine release response elicited by ACh (7). Figure 10E shows that the NACHRA3 was similarly expressed in the adrenal medullary tissue of WT and mSOD1 mice.

We also tested the expression of proteins in the brain cortex, the hippocampus and the spinal cord of WT and mSOD1 mice; the results are summarised in Figure 11. SYT1 density was similar in the cortex and the hippocampus and was poorly expressed in the spinal cord (panel A). This was also the case for VAMP2 that had about half density in the spinal cord, compared with the cortex and the hippocampus (panel D). STX1 and SNP25 were equally expressed in the three brain and spinal cord areas explored (panels B, C). Concerning WT and mSOD1 tissues, we found no differences in the expression of SYT1, STX1 and VAMP2 in the cortex, hippocampus and spinal cord (panels A, B, D). A 25% decrease of SNP25 expression was found in the spinal cord of mSOD1 mice, with respect to WT mice (panel C; $P < 0.05$). In WT mice, some regional statistically significant differences were found; for instance, STX1 expression was 35% lower in the hippocampus with respect to motor cortex (Figure 11B).

Motor deficits of mSOD1 with respect to WT mice

In this study we used WT and mSOD1 mice of ages between P90 and P130 days. At these ages the mutated mice show adult ALS onset (22, 23) and significant loss of vulnerable spinal motoneurons (9). Although motor impairment of mSOD1 at these ages is well documented we however explored the motor activity of the WT and mSOD1 mice used here, by means of the Rota-Rod test which assesses motor coordination and balance, as described by Jones and Roberts (28). Animals were placed on the rolling rod (32 mm diameter) with an initial speed of 8 rpm and an increase of 1 rpm each 8 seconds until they fell down; we made 2 measures of 10 repetitions: the training day (Trd) and the test day (Td), in two consecutive days, comparing WT and mSOD1 mice at P90 and P130 ages, as shown in Figure 12.

mSOD1 mice show a significant decrease in the time they stay on Rota-Rod compared to WT mice in both P90 (panel A, $P < 0.05$) and P130 (panel B, $P < 0.001$) as well as in both, Trds and Tds. Also, when comparing Trd and Td

646 we saw mSOD1 mice were not able to improve the time they stay on the rod at
647 both ages, in contrast with WT mice ($P < 0.01$). It is remarkable that mSOD1
648 mice show a significant 56% decrease of the time to fall in P130 compared with
649 P90 ($P < 0.05$), while WT mice show similar times (panel C).

DISCUSSION

In this study, pronounced alterations in cell excitability and ion currents, as well as in the kinetics of the exocytotic fusion pore have been found to occur in chromaffin cells from mSOD1, in comparison with WT mice. One of the most notable was the almost disappearance of spontaneous APs, an intrinsic property of chromaffin cells (12). The resting V_m in bisected mouse adrenal chromaffin cells using intracellular recordings *in situ* is 54.3 mV (42). Using the patch-clamp technique we have found here that WT and mSOD1 had somehow more hyperpolarised resting V_m, namely −68 mV and −63 mV, respectively. Considering that the resting V_m was at the same level in both cell types, the drastic difference in spontaneous firing may find an explanation in the depressed inward I_{Na} as well as in the outward $I_{K(Ca)}$ and $I_{K(V)}$ in mSOD1, with respect to WT cells, since these currents are known to contribute to the generation of APs in chromaffin cells (3, 5, 32, 39, 42).

Our results on depressed ion currents keep pace with those of the study of Boutahar et al. (4) dealing with the transcriptional profile of cortical neurons from E14 embryos of WT and mSOD1 mice. In mSOD1 neurons, the expression of Na^+ channel type VIIα (SNC7A) is depressed 7.2-fold and that of large-conductance Ca^{2+}-dependent K^+ channel (KCNMA1, BK channel) is depressed by 21-fold with respect to WT neurons. Also, in ALS patients immunoreactivity of Kv1.2 channels is markedly reduced in the ventral root (57). Furthermore, SH-SY5Y cells expressing the mutated $SOD1^{G93A}$ have a decreased I_{Na} (66). This depressed gene expression in cortical neurons support our conclusion that the depressed excitability of mSOD1 chromaffin cells is likely due to poorer expression of Na^+ and K^+ channels, thus explaining the decreased I_{Na} and I_K we found in these cells. A toxic gain of function has been considered the cause of motoneuron degeneration on mice overexpressing human mSOD1 (23). This hypothesis received support from a study on PC12 cells transfected with $SOD1^{G93A}$ that exhibit an increased production of hydroxyl radicals and an enhanced rate of apoptotic cell death (34). The possibility that this free radical overproduction is behind the alterations of cell excitability and

683 ion currents in mSOD1 chromaffin cells is worth of being explored in further
684 studies.
685
686 Bulk secretion of catecholamine measured as the total number of
687 individual spikes counted during the 1 minute stimulation with ACh, was similar
688 in both cell types. In principle, this agrees with the similar $[Ca^{2+}]_c$ transients
689 elicited by ACh, in spite of the fact I_{Ca} was mildly enhanced in mSOD1
690 chromaffin cells, in agreement with a previous study showing that N-type
691 VACCs were overexpressed in cortical neurons of mSOD1 mouse embryos
692 (49). However, if bulk secretion is measured as a summatory of all spike areas,
693 it came about that mSOD1 cells secreted 46.6% more catecholamine than WT
694 cells. This may be explained if the 52.24% higher Q of individual spikes is taken
695 into account. Similar $[Ca^{2+}]_c$ transients and secretion elicited by ACh are not in
696 agreement with the fact that I_{ACh} was 70% smaller in mSOD1 with respect to
697 WT cells. Because the protein expression of the α3 subunit of nicotinic
698 receptors is similar in both cell types, the 70% depressed I_{ACh} in mSOD1 cells
699 may be due to an altered receptor function. Compensatory overexpression of
700 other nicotinic receptor subtypes may also have occurred. This hypothesis
701 should be pursued in further studies.
702
703 An interesting difference was found in the kinetic parameters of the
704 exocytotic fusion pore, averaged from calculations done in thousands of
705 individual secretory amperometric spikes. These differences are as follows
706 (mSOD1 versus WT cells): 35.94% lower rise rate, 60.7% higher decay time,
707 55.3% higher $t_{1/2}$, 16.61% lower I_{max}, and 52.24% higher Q. This means that the
708 expansion of the fusion pore is slower, the release of vesicle contents takes
709 longer, and the release of catecholamine per vesicle is higher. In other words,
710 considering the 1 minute period of cell stimulation with ACh, the 21 vesicles that
711 undergo exocytosis in mSOD1 chromaffin cells release 50% more
712 catecholamine than the 24-25 vesicles of WT cells, but at a lower rate.
713
714 Probably, the more striking finding in this study is related to the fact that
715 the drastic differences in the secretion parameters found between WT and

716 mSOD1 cells when stimulated with ACh, were not present when cells were
717 stimulated with high K^+. Since long, ACh, high K^+, barium (Ba^{2+}), and several
718 other secretagogues have been used to trigger exocytosis and even to analyse
719 the kinetics of the fusion pore (37, 54). However, the physiological
720 neurotransmitter ACh (19) has been used more rarely simply because
721 chromaffin cells respond with a healthy secretory response with unphysiological
722 stimuli such as high K^+ or Ba^{2+} in a more reliable manner. As ACh, these stimuli
723 certainly cause cell depolarisation (47, 63). However, since the pioneering work
724 of William Douglas laboratory (16, 17), it has become clear that ACh and K^+
725 differ in their ability to trigger APs, $[Ca^{2+}]_c$ transients, and secretion. For
726 instance, according to the Nernst equation, high K^+ produces a sustained
727 depolarisation of chromaffin cells without superimposed APs (47). However,
728 ACh produces a mild depolarisation that serves to trigger APs in chromaffin
729 cells including mice (3, 5, 11, 12, 20, 26, 42). On the other hand, although ACh
730 and high K^+ elicit similar bulk secretory responses, the former causes more
731 localised and smaller $[Ca^{2+}]_c$ elevations and the latter evokes higher $[Ca^{2+}]_c$
732 transients that quickly spread out through the cytosol, as confocal microscopy
733 reveals (8).
734
735 In the light of those previous results, we may therefore conclude that
736 chromaffin cells challenged with ACh alters cell excitability and the ensuing
737 $[Ca^{2+}]_c$ transients and secretory responses, in a manner that considerably differ
738 from the responses elicited by sustained depolarisation with K^+. Massive Ca^{2+}
739 entry with high K^+ suggests that higher unbuffered $[Ca^{2+}]_c$ transients occur; this
740 is not the case for ACh that causes smaller and more localised $[Ca^{2+}]_c$
741 transients (8). This explains that high K^+ causes higher $[Ca^{2+}]_c$ transients in
742 mSOD1 cells, while the ACh $[Ca^{2+}]_c$ elevations are similar. Relevant to this
743 study is that the changes in the kinetics of the exocytotic fusion pore are only
744 present upon the physiological indirect depolarisation of chromaffin cells
745 through stimulation of their nicotinic receptors with ACh; those changes are not
746 seen with direct unphysiological stimulation with high K^+. This indicates that an
747 altered neurotransmission is present at the adrenal medulla of mSOD1 mice. It
748 will be interesting to test whether WT and mSOD1 mice respond differently to

cold or hypoglycemic stress before ALS-like disease starts and once the disease is established.

During the last two decades, the analysis of the distinct vesicle pools and of the pre-exocytotic and exocytotic events in chromaffin cells of transgenic mice, has been thoroughly applied to understand the molecular and cellular mechanisms involved in the exocytotic release of neurotransmitters (43, 58, 59). However, only recently similar studies are being performed in transgenic mouse models of neurodegenerative diseases. For instance, we found that in chromaffin cells of the APP/PS1 mouse model of AD, the exocytotic fusion pore closes faster and releases smaller amount of catecholamine but with a faster and more transient fusion pore opening, expansion and closure (13). This is just opposite to what we find here in the mSOD1 mouse model of ALS, where chromaffin cells exhibit a slower fusion pore kinetics but a greater release of catecholamine (see the two superimposed averaged AD and ALS secretory spike models in Figure 8F). The drastic different morphology of both spikes suggests they can serve as markers for ALS and AD. A recent study also indicates an alteration of pre-exocytotic and exocytotic steps in chromaffin cells of a mouse model of HD; this study concludes that the HAP1 regulates exocytosis via two potentially interlinked mechanisms: control of vesicle docking and the size of the RRP, and the regulation of fusion pore stabilisation (35).

In conclusion, we present here the first study showing a drastic change in the kinetics of the exocytotic fusion pore in chromaffin cells from the mSOD1 mouse model of ALS, with respect to WT mice, when physiologically challenged with ACh. A slower fusion pore opening, expansion, and closure is likely due to a pronounced reduction of cell excitability and ion currents driving APs in mSOD1 chromaffin cells. These changes may help to better understand human ALS pathogenesis and to inspire novel biological targets for the eventual development of a medicine to treat patients suffering of intractable ALS.

ACKNOWLEDGEMENTS

We appreciate the continued support of Fundación Teófilo Hernando.

José-Carlos Fernández-Morales present address: Department of Cell Biology, Medical University of South Carolina, Charleston, SC 29403, USA.

Antonio M. G. de Diego present address: Ear Institute, University College London, London WC1E 6BT, UK.

FUNDING & GRANTS

This work was funded by: (1) SAF-2010-21795, MINECO; (2) SAF-2010-18837, MINECO; (3) CABICYC, UAM/Bioibérica; (4) Fundación Teófilo Hernando, Madrid, Spain.

DISCLOSURES

The authors declare no competing financial interests.

800 REFERENCES

801

802 1. **Baker PF, and Knight DE**. Calcium-dependent exocytosis in bovine
803 adrenal medullary cells with leaky plasma membranes. *Nature* 276: 620-622,
804 1978.
805 2. **Bensimon G, Lacomblez L, and Meininger V**. A controlled trial of
806 riluzole in amyotrophic lateral sclerosis. ALS/Riluzole Study Group. *N Engl J*
807 *Med* 330: 585-591, 1994.
808 3. **Biales B, Dichter M, and Tischler A**. Electrical excitability of cultured
809 adrenal chromaffin cells. *J Physiol* 262: 743-753, 1976.
810 4. **Boutahar N, Wierinckx A, Camdessanche JP, Antoine JC, Reynaud**
811 **E, Lassabliere F, Lachuer J, and Borg J**. Differential effect of oxidative or
812 excitotoxic stress on the transcriptional profile of amyotrophic lateral sclerosis-
813 linked mutant SOD1 cultured neurons. *J Neurosci Res* 89: 1439-1450, 2011.
814 5. **Brandt BL, Hagiwara S, Kidokoro Y, and Miyazaki S**. Action potentials
815 in the rat chromaffin cell and effects of acetylcholine. *J Physiol* 263: 417-439,
816 1976.
817 6. **Couratier P, Hugon J, Sindou P, Vallat JM, and Dumas M**. Cell culture
818 evidence for neuronal degeneration in amyotrophic lateral sclerosis being linked
819 to glutamate AMPA/kainate receptors. *Lancet* 341: 265-268, 1993.
820 7. **Criado M, Alamo L, and Navarro A**. Primary structure of an agonist
821 binding subunit of the nicotinic acetylcholine receptor from bovine adrenal
822 chromaffin cells. *Neurochem Res* 17: 281-287, 1992.
823 8. **Cuchillo-Ibanez I, Olivares R, Aldea M, Villarroya M, Arroyo G,**
824 **Fuentealba J, Garcia AG, and Albillos A**. Acetylcholine and potassium elicit
825 different patterns of exocytosis in chromaffin cells when the intracellular calcium
826 handling is disturbed. *Pflugers Arch* 444: 133-142, 2002.
827 9. **Chiu AY, Zhai P, Dal Canto MC, Peters TM, Kwon YW, Prattis SM,**
828 **and Gurney ME**. Age-dependent penetrance of disease in a transgenic mouse
829 model of familial amyotrophic lateral sclerosis. *Mol Cell Neurosci* 6: 349-362,
830 1995.

831 10. **Chow RH, von Ruden L, and Neher E**. Delay in vesicle fusion revealed
832 by electrochemical monitoring of single secretory events in adrenal chromaffin
833 cells. *Nature* 356: 60-63, 1992.
834 11. **de Diego AM**. Electrophysiological and morphological features
835 underlying neurotransmission efficacy at the splanchnic nerve-chromaffin cell
836 synapse of bovine adrenal medulla. *Am J Physiol Cell Physiol* 298: C397-405,
837 2009.
838 12. **de Diego AM, Gandia L, and Garcia AG**. A physiological view of the
839 central and peripheral mechanisms that regulate the release of catecholamines
840 at the adrenal medulla. *Acta Physiol (Oxf)* 192: 287-301, 2008.
841 13. **de Diego AM, Lorrio S, Calvo-Gallardo E, and Garcia AG**. Smaller
842 quantal size and faster kinetics of single exocytotic events in chromaffin cells
843 from the APP/PS1 mouse model of Alzheimer's disease. *Biochem Biophys Res*
844 *Commun* 428: 482-486, 2012.
845 14. **Delestree N, Manuel M, Iglesias C, Elbasiouny SM, Heckman CJ, and**
846 **Zytnicki D**. Adult spinal motoneurones are not hyperexcitable in a mouse
847 model of inherited amyotrophic lateral sclerosis. *J Physiol* 592: 1687-1703,
848 2014.
849 15. **Douglas WW, and Poisner AM**. Stimulation of uptake of calcium-45 in
850 the adrenal gland by acetylcholine. *Nature* 192: 1299, 1961.
851 16. **Douglas WW, and Rubin RP**. The mechanism of catecholamine release
852 from the adrenal medulla and the role of calcium in stimulus-secretion coupling.
853 *J Physiol* 167: 288-310, 1963.
854 17. **Douglas WW, and Rubin RP**. The role of calcium in the secretory
855 response of the adrenal medulla to acetylcholine. *J Physiol* 159: 40-57, 1961.
856 18. **Feissner RF, Skalska J, Gaum WE, and Sheu SS**. Crosstalk signaling
857 between mitochondrial Ca2+ and ROS. *Front Biosci* 14: 1197-1218, 2009.
858 19. **Feldberg W, Minz B, and Tsudzimura H**. The mechanism of the
859 nervous discharge of adrenaline. *J Physiol* 81: 286-304, 1934.
860 20. **Fenwick EM, Marty A, and Neher E**. A patch-clamp study of bovine
861 chromaffin cells and of their sensitivity to acetylcholine. *J Physiol* 331: 577-597,
862 1982.

21. **Fernandez-Morales JC, Cortes-Gil L, Garcia AG, and de Diego AM**. Differences in the quantal release of catecholamines in chromaffin cells of rat embryos and their mothers. *Am J Physiol Cell Physiol* 297: C407-418, 2009.

22. **Fuchs A, Ringer C, Bilkei-Gorzo A, Weihe E, Roeper J, and Schutz B**. Downregulation of the potassium chloride cotransporter KCC2 in vulnerable motoneurons in the SOD1-G93A mouse model of amyotrophic lateral sclerosis. *J Neuropathol Exp Neurol* 69: 1057-1070, 2010.

23. **Gurney ME, Pu H, Chiu AY, Dal Canto MC, Polchow CY, Alexander DD, Caliendo J, Hentati A, Kwon YW, Deng HX, and et al.** Motor neuron degeneration in mice that express a human Cu,Zn superoxide dismutase mutation. *Science* 264: 1772-1775, 1994.

24. **Hamill OP, Marty A, Neher E, Sakmann B, and Sigworth FJ**. Improved patch-clamp techniques for high-resolution current recording from cells and cell-free membrane patches. *Pflugers Arch* 391: 85-100, 1981.

25. **Hernandez-Guijo JM, Maneu-Flores VE, Ruiz-Nuno A, Villarroya M, Garcia AG, and Gandia L**. Calcium-dependent inhibition of L, N, and P/Q Ca2+ channels in chromaffin cells: role of mitochondria. *J Neurosci* 21: 2553-2560, 2001.

26. **Holman ME, Coleman HA, Tonta MA, and Parkington HC**. Synaptic transmission from splanchnic nerves to the adrenal medulla of guinea-pigs. *J Physiol* 478 (Pt 1): 115-124, 1994.

27. **Ilieva H, Polymenidou M, and Cleveland DW**. Non-cell autonomous toxicity in neurodegenerative disorders: ALS and beyond. *J Cell Biol* 187: 761-772, 2009.

28. **Jones BJ, and Roberts DJ**. The quantiative measurement of motor inco-ordination in naive mice using an acelerating rotarod. *J Pharm Pharmacol* 20: 302-304, 1968.

29. **Katz B, and Thesleff S**. A study of the desensitization produced by acetylcholine at the motor end-plate. *J Physiol* 138: 63-80, 1957.

30. **Kawagoe KT, Zimmerman JB, and Wightman RM**. Principles of voltammetry and microelectrode surface states. *J Neurosci Methods* 48: 225-240, 1993.

31. **Kawahara Y, Ito K, Sun H, Aizawa H, Kanazawa I, and Kwak S**. Glutamate receptors: RNA editing and death of motor neurons. *Nature* 427: 801, 2004.

32. **Kidokoro Y, and Ritchie AK**. Chromaffin cell action potentials and their possible role in adrenaline secretion from rat adrenal medulla. *J Physiol* 307: 199-216, 1980.

33. **Kuo JJ, Siddique T, Fu R, and Heckman CJ**. Increased persistent Na(+) current and its effect on excitability in motoneurones cultured from mutant SOD1 mice. *J Physiol* 563: 843-854, 2005.

34. **Liu R, Narla RK, Kurinov I, Li B, and Uckun FM**. Increased hydroxyl radical production and apoptosis in PC12 neuron cells expressing the gain-of-function mutant G93A SOD1 gene. *Radiat Res* 151: 133-141, 1999.

35. **Mackenzie KD, Duffield MD, Peiris H, Phillips L, Zanin MP, Teo EH, Zhou XF, and Keating DJ**. Huntingtin-associated protein 1 regulates exocytosis, vesicle docking, readily releasable pool size and fusion pore stability in mouse chromaffin cells. *J Physiol* 2014.

36. **Machado DJ, Montesinos MS, and Borges R**. Good practices in single-cell amperometry. *Methods Mol Biol* 440: 297-313, 2008.

37. **Machado JD, Segura F, Brioso MA, and Borges R**. Nitric oxide modulates a late step of exocytosis. *J Biol Chem* 275: 20274-20279, 2000.

38. **Martin D, Thompson MA, and Nadler JV**. The neuroprotective agent riluzole inhibits release of glutamate and aspartate from slices of hippocampal area CA1. *Eur J Pharmacol* 250: 473-476, 1993.

39. **Marty A**. Ca-dependent K channels with large unitary conductance in chromaffin cell membranes. *Nature* 291: 497-500, 1981.

40. **Miranda-Ferreira R, de Pascual R, de Diego AM, Caricati-Neto A, Gandia L, Jurkiewicz A, and Garcia AG**. Single-vesicle catecholamine release has greater quantal content and faster kinetics in chromaffin cells from hypertensive, as compared with normotensive, rats. *J Pharmacol Exp Ther* 324: 685-693, 2008.

41. **Mosharov EV, and Sulzer D**. Analysis of exocytotic events recorded by amperometry. *Nat Methods* 2: 651-658, 2005.

927 42. **Nassar-Gentina V, Pollard HB, and Rojas E**. Electrical activity in
928 chromaffin cells of intact mouse adrenal gland. *Am J Physiol* 254: C675-683,
929 1988.
930 43. **Neher E**. Vesicle pools and Ca2+ microdomains: new tools for
931 understanding their roles in neurotransmitter release. *Neuron* 20: 389-399,
932 1998.
933 44. **Nicholls DG**. Oxidative stress and energy crises in neuronal dysfunction.
934 *Ann N Y Acad Sci* 1147: 53-60, 2008.
935 45. **Nistri A, and Cherubini E**. Inactivation characteristics of a sustained,
936 Ca(2+)-independent K+ current of rat hippocampal neurones in vitro. *J Physiol*
937 457: 575-590, 1992.
938 46. **Ochoa EL, Chattopadhyay A, and McNamee MG**. Desensitization of
939 the nicotinic acetylcholine receptor: molecular mechanisms and effect of
940 modulators. *Cell Mol Neurobiol* 9: 141-178, 1989.
941 47. **Orozco C, Garcia-de-Diego AM, Arias E, Hernandez-Guijo JM, Garcia**
942 **AG, Villarroya M, and Lopez MG**. Depolarization preconditioning produces
943 cytoprotection against veratridine-induced chromaffin cell death. *Eur J*
944 *Pharmacol* 553: 28-38, 2006.
945 48. **Pieri M, Albo F, Gaetti C, Spalloni A, Bengtson CP, Longone P,**
946 **Cavalcanti S, and Zona C**. Altered excitability of motor neurons in a transgenic
947 mouse model of familial amyotrophic lateral sclerosis. *Neurosci Lett* 351: 153-
948 156, 2003.
949 49. **Pieri M, Caioli S, Canu N, Mercuri NB, Guatteo E, and Zona C**. Over-
950 expression of N-type calcium channels in cortical neurons from a mouse model
951 of Amyotrophic Lateral Sclerosis. *Exp Neurol* 247: 349-358, 2013.
952 50. **Pieri M, Carunchio I, Curcio L, Mercuri NB, and Zona C**. Increased
953 persistent sodium current determines cortical hyperexcitability in a genetic
954 model of amyotrophic lateral sclerosis. *Exp Neurol* 215: 368-379, 2009.
955 51. **Quinlan KA, Schuster JE, Fu R, Siddique T, and Heckman CJ**.
956 Altered postnatal maturation of electrical properties in spinal motoneurons in a
957 mouse model of amyotrophic lateral sclerosis. *J Physiol* 589: 2245-2260, 2011.
958 52. **Rothstein JD**. Of mice and men: reconciling preclinical ALS mouse
959 studies and human clinical trials. *Ann Neurol* 53: 423-426, 2003.

960 53. **Rowland LP, and Shneider NA**. Amyotrophic lateral sclerosis. *N Engl J*
961 *Med* 344: 1688-1700, 2001.
962 54. **Schroeder TJ, Borges R, Finnegan JM, Pihel K, Amatore C, and**
963 **Wightman RM**. Temporally resolved, independent stages of individual
964 exocytotic secretion events. *Biophys J* 70: 1061-1068, 1996.
965 55. **Segovia M, Ales E, Montes MA, Bonifas I, Jemal I, Lindau M,**
966 **Maximov A, Sudhof TC, and Alvarez de Toledo G**. Push-and-pull regulation
967 of the fusion pore by synaptotagmin-7. *Proc Natl Acad Sci U S A* 107: 19032-
968 19037, 2010.
969 56. **Shaw PJ, and Eggett CJ**. Molecular factors underlying selective
970 vulnerability of motor neurons to neurodegeneration in amyotrophic lateral
971 sclerosis. *J Neurol* 247 Suppl 1: I17-27, 2000.
972 57. **Shibuya K, Misawa S, Arai K, Nakata M, Kanai K, Yoshiyama Y, Ito**
973 **K, Isose S, Noto Y, Nasu S, Sekiguchi Y, Fujimaki Y, Ohmori S, Kitamura**
974 **H, Sato Y, and Kuwabara S**. Markedly reduced axonal potassium channel
975 expression in human sporadic amyotrophic lateral sclerosis: an
976 immunohistochemical study. *Exp Neurol* 232: 149-153, 2011.
977 58. **Sorensen JB**. Formation, stabilisation and fusion of the readily
978 releasable pool of secretory vesicles. *Pflugers Arch* 448: 347-362, 2004.
979 59. **Sudhof TC**. The synaptic vesicle cycle. *Annu Rev Neurosci* 27: 509-547,
980 2004.
981 60. **Tateno M, Sadakata H, Tanaka M, Itohara S, Shin RM, Miura M,**
982 **Masuda M, Aosaki T, Urushitani M, Misawa H, and Takahashi R**. Calcium-
983 permeable AMPA receptors promote misfolding of mutant SOD1 protein and
984 development of amyotrophic lateral sclerosis in a transgenic mouse model.
985 *Hum Mol Genet* 13: 2183-2196, 2004.
986 61. **Villarroya M, Olivares R, Ruiz A, Cano-Abad MF, de Pascual R,**
987 **Lomax RB, Lopez MG, Mayorgas I, Gandia L, and Garcia AG**. Voltage
988 inactivation of Ca2+ entry and secretion associated with N- and P/Q-type but
989 not L-type Ca2+ channels of bovine chromaffin cells. *J Physiol* 516 (Pt 2): 421-
990 432, 1999.

991 62. **von Lewinski F, and Keller BU**. Ca2+, mitochondria and selective
992 motoneuron vulnerability: implications for ALS. *Trends Neurosci* 28: 494-500,
993 2005.
994 63. **von Ruden L, Garcia AG, and Lopez MG**. The mechanism of Ba(2+)-
995 induced exocytosis from single chromaffin cells. *FEBS Lett* 336: 48-52, 1993.
996 64. **Wightman RM, Jankowski JA, Kennedy RT, Kawagoe KT, Schroeder**
997 **TJ, Leszczyszyn DJ, Near JA, Diliberto EJ, Jr., and Viveros OH**. Temporally
998 resolved catecholamine spikes correspond to single vesicle release from
999 individual chromaffin cells. *Proc Natl Acad Sci U S A* 88: 10754-10758, 1991.
1000 65. **Yanez M, Galan L, Matias-Guiu J, Vela A, Guerrero A, and Garcia**
1001 **AG**. CSF from amyotrophic lateral sclerosis patients produces glutamate
1002 independent death of rat motor brain cortical neurons: protection by resveratrol
1003 but not riluzole. *Brain Res* 1423: 77-86, 2011.
1004 66. **Zona C, Ferri A, Gabbianelli R, Mercuri NB, Bernardi G, Rotilio G,**
1005 **and Carri MT**. Voltage-activated sodium currents in a cell line expressing a
1006 Cu,Zn superoxide dismutase typical of familial ALS. *Neuroreport* 9: 3515-3518,
1007 1998.
1008

1009 FIGURE LEGENDS

1010

1011 FIGURE 1.

1012 Drastic reduction in the number of spontaneous action potentials in mSOD1

1013 chromaffin cells compared with WT cells.

1014

1015 A, example voltage record obtained from a WT cell. B, voltage record

1016 obtained from an example mSOD1 cell. C, average action potential

1017 number recount from 300 s records of WT and mSOD1 cells. D, average

1018 resting membrane potentials from WT and mSOD1 cells. Data in C and D

1019 are means ± SEM of the number of cells and cultures shown in

1020 parentheses. ***P < 0.001 with respect to WT cells (unpaired Student's t-

1021 test).

1022

1023 FIGURE 2.

1024 Nicotinic (I_{ACh}) and potassium currents (I_K) were markedly diminished in voltage-

1025 clamped chromaffin cells from mSOD1 mice, with respect to those from WT

1026 mice.

1027

1028 Whole-cell inward nicotinic currents (I_{ACh}) were generated by 250-ms

1029 pulses of 100 µM ACh, applied to cells voltage-clamped at −80 mV at 2-

1030 min intervals. Outward K^+ currents (I_K) were recorded in cells voltage-

1031 clamped at −80 mV and challenged first with a 10-ms depolarising pulse

1032 to +30 mV to elicit calcium currents (I_{Ca}), and subsequently with a 400-

1033 ms depolarising pulse to +120 mV to evoke I_K (protocol in panel 2E). A,

1034 I_{ACh} traces obtained in an example WT cell. B, I_{ACh} traces obtained in an

1035 example mSOD1 cell. C, superimposed I_{ACh} traces of an example WT

1036 cell (dark trace) and mSOD1 cell (light trace). D, averaged peak

1037 amplitude of I_{ACh} in WT and mSOD1 cells. E, I_K traces from an example

1038 WT (dark trace) and mSOD1 (light trace) cells exhibiting a large transient

1039 calcium-dependent K^+ current ($I_{K(Ca)}$) and a smaller non-inactivating

1040 plateau voltage-dependent K^+ current ($I_{K(V)}$); the pre-pulse and test pulse

1041 protocol are shown on top. F, average results of the amplitudes of the I_K

components, $I_{K(Ca)}$ and $I_{K(V)}$ in both cell types. Data in D and F are means ± SEM of the number of cells and cultures shown in parentheses. ***P* < 0.01, ****P* < 0.001 with respect to WT cells (unpaired Student's t-test).

FIGURE 3.

Augmentation of the whole-cell inward calcium current (I_{Ca}) and reduction of the whole-cell inward sodium current (I_{Na}) in mSOD1 chromaffin cells, with respect to WT cells.

To elicit calcium (I_{Ca}) and sodium (I_{Na}) currents cells were voltage-clamped at −80 mV and stimulated with 50-ms test depolarising pulses to −10 or 0 mV for I_{Ca} and with 10-ms test depolarising pulses to –10 mV for I_{Na}. A, I_{Ca} traces of an example WT (dark trace) and mSOD1 (light trace) cells. B, averaged peak amplitude of I_{Ca} in WT and mSOD1 cells. C, I_{Na} traces of an example WT (dark trace) and mSOD1 (light trace) cells. D, averaged peak amplitude of I_{Na} in WT and mSOD1 cells. Data in B and D are means ± SEM of the number of cells and cultures shown in parentheses. ***P* < 0.01 with respect to WT cells (unpaired Student's t-test).

FIGURE 4.

Elevations of the cytosolic Ca^{2+} concentrations ($[Ca^{2+}]_c$) elicited by 1 min challenging with acetylcholine (ACh) of high potassium (K^+) in WT and mSOD1 chromaffin cells.

Fura-2AM loaded cells were perifused for 1 min with saline solutions containing 100 µM ACh (A) or 75 mM K^+ (low Na^+, B), as indicated by horizontal lines at the bottom. A and B, overlapping $[Ca^{2+}]_c$ traces (expressed as arbitrary fluorescence units, AFU) obtained in example WT and mSOD1 cells. Averaged pooled results of time to peak of the $[Ca^{2+}]_c$ elevation (C), peak amplitude (D) and area (E) as indication of the total $[Ca^{2+}]_c$ transient of WT and mSOD1 cells. Data are means ± SEM of the number of cells shown in parentheses on top of panel C, from at least

3 different cultures. ***$P < 0.001$ (one-way ANOVA test and Tukey post-hoc analyses).

FIGURE 5.

Higher total catecholamine release in mSOD1 chromaffin cells compared with WT cells stimulated with acetylcholine (ACh).

A, example record obtained from a WT cell stimulated with 100 µM ACh for 1 min (bottom horizontal bar). B, record obtained from an example mSOD1 cell similarly stimulated with ACh. C, cumulative secretion calculated at 5 s intervals in traces similar to those shown in A and B; the area of spikes is expressed in pC (ordinate) as a function of time (abscissa). D, secretion per stimulation period (integrated area of all spikes generated by the ACh pulse) in pC (ordinate). E, total number of spikes secreted per each ACh pulse (ordinate). F, quantal size of individual secretory events expressed in pC (ordinate). Data in C, D, E are means ± SEM of the number of cells and cultures shown in parentheses. Data in F are means ± SEM of the number of individual spikes shown in parentheses; those spikes are from the experiments of D and E. *$P < 0.05$, ***$P < 0.001$ with respect to WT cells (unpaired Student's t-test).

FIGURE 6.

Similar total catecholamine release in mSOD1 chromaffin cells compared with WT cells stimulated with high potassium (K^+).

A, example record obtained from a WT cell stimulated with 75 mM K^+ (low Na^+) for 1 min (bottom horizontal bar). B, record obtained from an example mSOD1 cell similarly stimulated with K^+. C, cumulative secretion calculated at 5 s intervals in traces similar to those shown in A and B; the area of spikes is expressed in pC (ordinate) as a function of time (abscissa). D, secretion per stimulation period (integrated area of all spikes generated by the K^+ pulse) in pC (ordinate). E, total number of

spikes secreted per each K^+ pulse (ordinate). F, quantal size of individual secretory events expressed in pC (ordinate). Data in C, D and E are means ± SEM of the number of cells and cell cultures shown in parentheses. Data in F are means ± SEM of the number of individual spikes shown in parentheses; those spikes are from the experiments of D and E. There are no significant differences between WT and mSOD1 cells (unpaired Student's t-test).

FIGURE 7.

Histograms of spike frequency versus time analysed on secretory traces obtained from WT and mSOD1 chromaffin cells stimulated with acetylcholine (ACh) or high potassium (K^+).

A,B, frequency histograms of spike frequency (ordinates) versus time (abscissa) challenged with ACh in WT and mSOD1 cells. C,D, frequency histograms of spike frequency (ordinates) versus time (abscissa) challenged with 75 mM K^+ (low Na^+) in WT and mSOD1 cells. E, time constant for inactivation (τ_i, ordinate in seconds) calculated from the decay of spike frequency of panels A,B,C,D. Data in panel E are means ± SEM of the number of cells and cell cultures shown in parentheses in panels A to D. *P < 0.05 (unpaired Student's t-test).

FIGURE 8.

Prototype spike shapes obtained from averaged pooled data on the kinetic parameters of individual exocytotic spike events taken from experiments of Figures 5 and 6 and summarised in Table 1, done in chromaffin cells from WT and mSOD1 mice.

A, spike model showing the kinetic parameters calculated for the foot (Table 3) and the spike (Table 1). B, superimposed averaged spikes for WT (continuous line) and mSOD1 cells (discontinuous line) stimulated with ACh (100 μM); C, superimposed averaged spikes for cells of WT (continuous line) and mSOD1 (discontinuous line) stimulated with K^+ (75

mM, low Na^+); D, superimposed averaged spikes for WT cells stimulated with ACh (continuous line) or K^+ (discontinuous line); E, superimposed averaged spikes for mSOD1 cells stimulated with ACh (continuous line) and K^+ (discontinuous line). F, overlapping averaged spikes from chromaffin cells from APP/PS1 mice model of AD (discontinuous line, taken from de Diego et al., 2012) and an ALS mouse model (continuous line, from this study).

FIGURE 9.

Types of secretory spike events in chromaffin cells from WT and mSOD1 mice stimulated with ACh or K^+.

Example spike events were selected from secretory traces from experiments of Figures 5 and 6. A, spike with foot (left) and stand-alone spike (right) of a WT cell stimulated with ACh (100 µM); B, overlapping spikes in a WT cell stimulated with ACh; C, overlapping spikes and partial fusion pore (flicker) followed by a spike (full fusion pore) of a WT cell stimulated with K^+ (75 mM, low Na^+); D, spike with foot (left) and stand-alone spike of a mSOD1 cell stimulated with ACh (right); E, transient fusion pore (flicker) and overlapping spikes of a mSOD1 cell stimulated with ACh; F, flicker and overlapping spikes in a mSOD1 cell stimulated with K^+. Quantitative pooled data on the frequency of these exocytotic spike events are summarised in Table 2.

FIGURE 10.

Relative expression of proteins of the exocytotic machinery and the α3 subunit of nicotinic receptors in adrenal medullary tissue from WT and mSOD1 mice, monitored with western blot.

An immunoblot from a representative experiment is shown on the top of each panel. Top bands correspond to synaptotagmin 7 (SYT7, panel A), syntaxin 1 (STX1, panel B), synaptosomal-associated protein 25 1 (SNP25, panel C), vesicle-associated membrane protein 2 (VAMP2,

panel D) and neuronal acetylcholine receptor subunit α3 (NACHRA3, panel E); lower bands correspond to control β-actin (ACTB). Bar diagrams represent pooled averaged results of adrenal glands from WT and mSOD1 mice. The relative band densities were calculated as ratios between the density of each band protein and its corresponding ACTB band, within each individual immunoblot. Values are means ± SEM. There are not significant differences between WT and mSOD1 mice (unpaired Student's t-test).

FIGURE 11.

Relative expression of proteins of the exocytotic machinery and the α3 subunit of nicotinic receptors in the motor cortex, the hippocampus and the spinal cord from WT and mSOD1 mice, monitored with western blot.

An immunoblot from a representative experiment is shown on the top of each panel. Top bands correspond to synaptotagmin 1 (SYT1, panel A), syntaxin 1 (STX1, panel B), synaptosomal-associated protein 25 1 (SNP25, panel C), vesicle-associated membrane protein 2 (VAMP2, panel D) and neuronal acetylcholine receptor subunit α3 (NACHRA3, panel E); lower bands correspond to control β-actin (ACTB). Bar diagrams represent pooled averaged results motor cortex, hippocampus and spinal cord from WT and mSOD1 mice. The relative band densities were calculated as ratios between the density of each band protein and its corresponding ACTB band, within each individual immunoblot. Values are means ± SEM. $*P < 0.05$, $**P < 0.01$, $***P < 0.001$ (one-way ANOVA/Newmann-Keuls); $^{\#}P < 0.05$ (unpaired Student's t-test).

FIGURE 12.

Time standing on Rota-Rod diminishes in mSOD1 mice with respect to WT mice and is age-dependent.

Mice were placed onto Rota-Rod and challenged with an initial speed of 8 rpm and an increase of 1 rpm each 8 seconds until they fell down; we

made 2 measures of 10 repetitions: during the training day (Trd) and the test day (Td), in two consecutive days. A, WT (white bars) and mSOD1 (black bars) mice used were at postnatal day 90 comparing Trd (stripped bars) and Td (plain bars). B, WT (white bars) and mSOD1 (black bars) mice used were at postnatal day 130 comparing Trd (stripped bars) and Td (plain bars). C, Comparison between Tds of WT (white bars) and mSOD1 (black bars) mice. Data are means ± SEM of the number of mice shown in parentheses. $*P < 0.05$, $**P < 0.01$, $***P < 0.001$ (unpaired Student's t-test).

TABLE LEGENDS

TABLE 1.

Single spike kinetic parameters calculated from the secretory traces obtained in WT and mSOD1 chromaffin cells stimulated with ACh (100 µM) or K^+ (75 mM) for 1 min.

Individual spike data in each cell were analysed and averaged; hence, final averaged data are expressed as the means of all cells (in parentheses). Rise rate was calculated with the slope of the ascending spike phase; decay time was calculated from the time between 75% and 25% of spike height in the descending spike phase; $t_{1/2}$ is the width of the spike at 50% of spike height; I_{max} is the height of the spike; Q is the spike area, an indication of catecholamine vesicle content and release (quantal size). Chromaffin cells from WT and mSOD1 mice were compared for each single spike parameter (columns) using the nonparametric Mann-Whitney rank sum test. Significant differences between both cell types are symbolised with asterisks in the mSOD1 row. Data are presented as means ± SEM with relative change of mSOD1 respect to WT (in mSOD1-ACh row) or relative change of K^+ respect to ACh (in K^+ rows) given in parentheses. Statistical tests were performed using the mean of at least 10 spikes per cell for each parameter. *P < 0.05, **P < 0.01, ***P < 0.001 in mSOD1 with respect to WT chromaffin cells for each stimulus; $^{\#}P$ < 0.05, $^{\#\#}P$ < 0.01, $^{\#\#\#}P$ < 0.001 in K^+ with respect to ACh stimulus for each cell type (unpaired Student's t-test in both cases).

TABLE 2.

Characteristics of exocytotic spike events in WT and mSOD1 chromaffin cells stimulated with ACh (100 µM) or K^+ (75 mM) for 1 min.

Data were obtained through the manual analysis of secretory event traces obtained from experiments shown in Figures 5A,B (ACh) and 6A,B (K^+), counting the different types of events as displayed in Figure 9. Data

are presented as means ± SEM with relative change of mSOD1 respect to WT (in mSOD1-ACh row) or relative change of K^+ respect to ACh (in K^+ rows) given in parentheses. *P < 0.05 in mSOD1 with respect to WT chromaffin cells for each stimulus; $^{\#\#}P$ < 0.01 in K^+ with respect to ACh stimulus for each cell type (unpaired Student's t-test in both cases).

TABLE 3.

Kinetic parameters of feet found at the beginning of single amperometric events in the secretory traces obtained in WT and mSOD1 chromaffin cells stimulated with ACh (100 µM) or K^+ (75 mM) for 1 min.

t_{foot} is the duration of the foot, I_{foot} is foot height; Q_{foot} is the area of the foot (catecholamine release during the foot). Chromaffin cells from WT and mSOD1 mice were compared for each single-spike foot parameter (columns) using the nonparametric Mann-Whitney rank sum test. Significant differences between both cell types are symbolised with asterisks in the mSOD1 row. Data are presented as means ± SEM with relative change of mSOD1 respect to WT (in mSOD1-ACh row) or relative change of K^+ respect to ACh (in K^+ rows) given in parentheses. Statistical tests were performed using the mean of at least 10 spikes per cell for each parameter. *P < 0.05, ***P < 0.001 in mSOD1 with respect to WT chromaffin cells for each stimulus; $^{\#}P$ < 0.05, $^{\#\#}P$ < 0.01, $^{\#\#\#}P$ < 0.001 in K^+ with respect to ACh stimulus for each cell type (unpaired Student's t-test in both cases).

FIGURES

FIGURE 1.

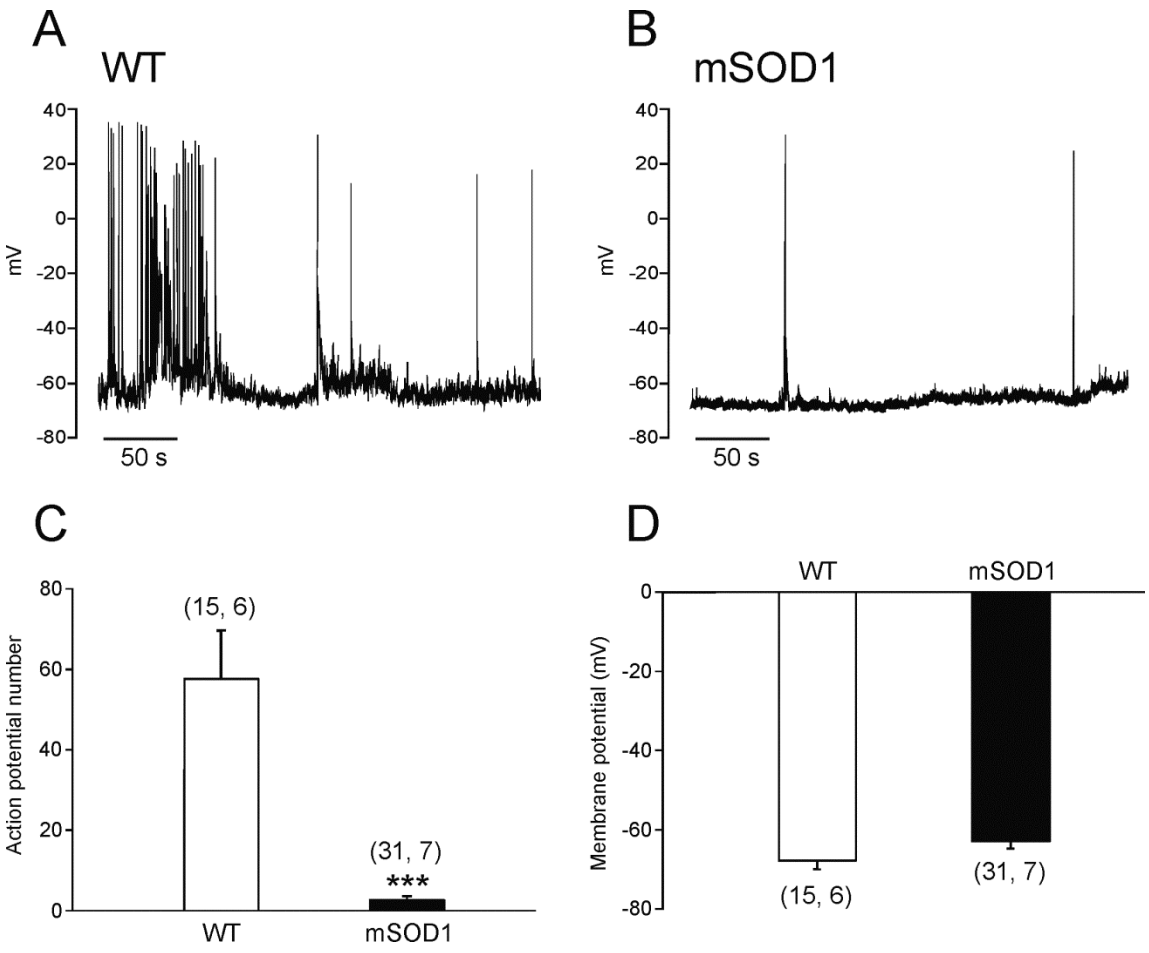

FIGURE 2.

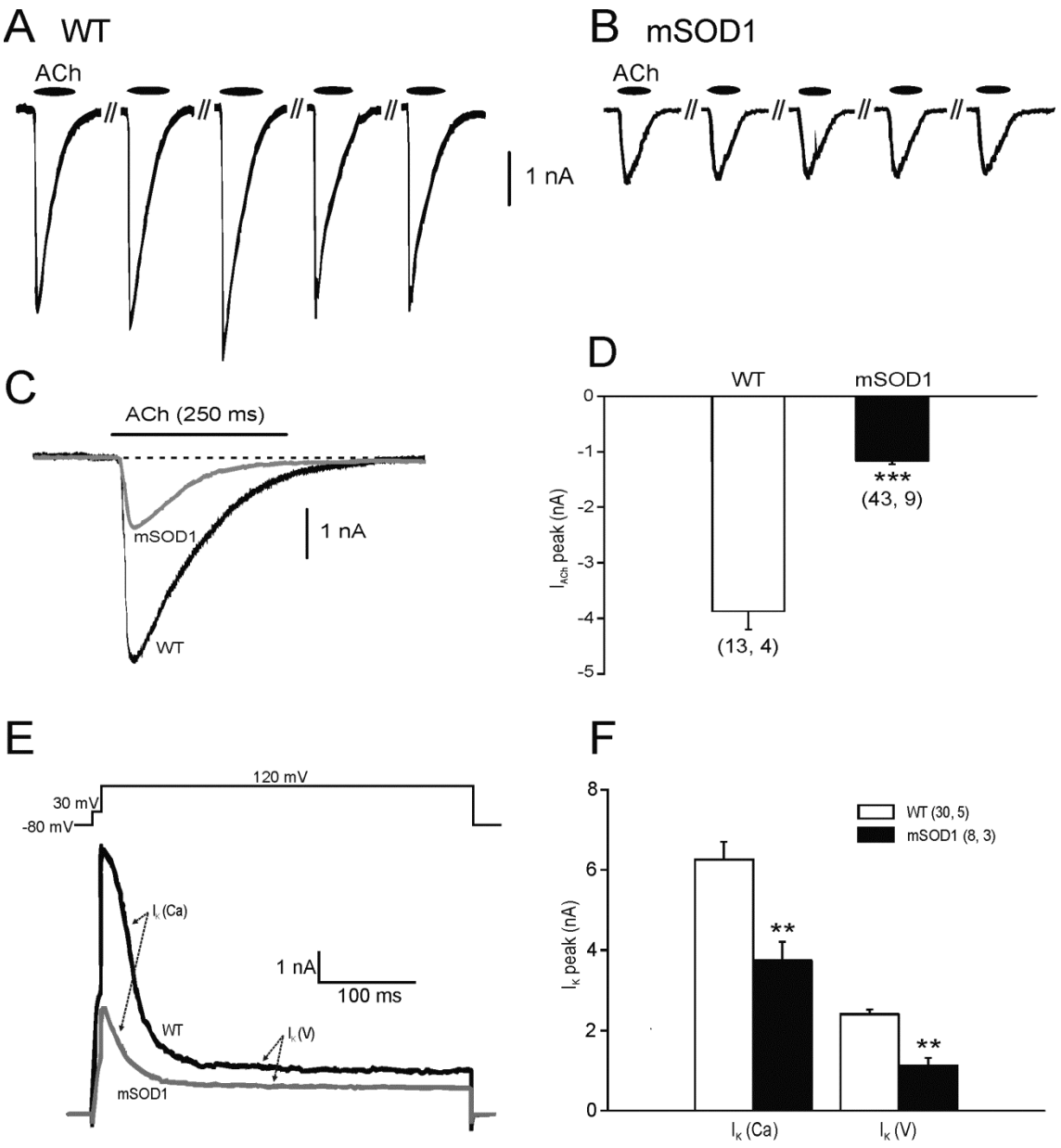
A WT
ACh
1 nA
B mSOD1
ACh
C
ACh (250 ms)
mSOD1
1 nA
WT
D
WT
mSOD1
0
-1
-2
-3
-4
-5
I_{ACh} peak (nA)
***
(43, 9)
(13, 4)
E
120 mV
30 mV
-80 mV
I_k (Ca)
1 nA
100 ms
WT
I_k (V)
mSOD1
F
WT (30, 5)
mSOD1 (8, 3)
8
6
4
2
0
I_k peak (nA)
**
**
I_k (Ca)
I_k (V)

FIGURE 3.

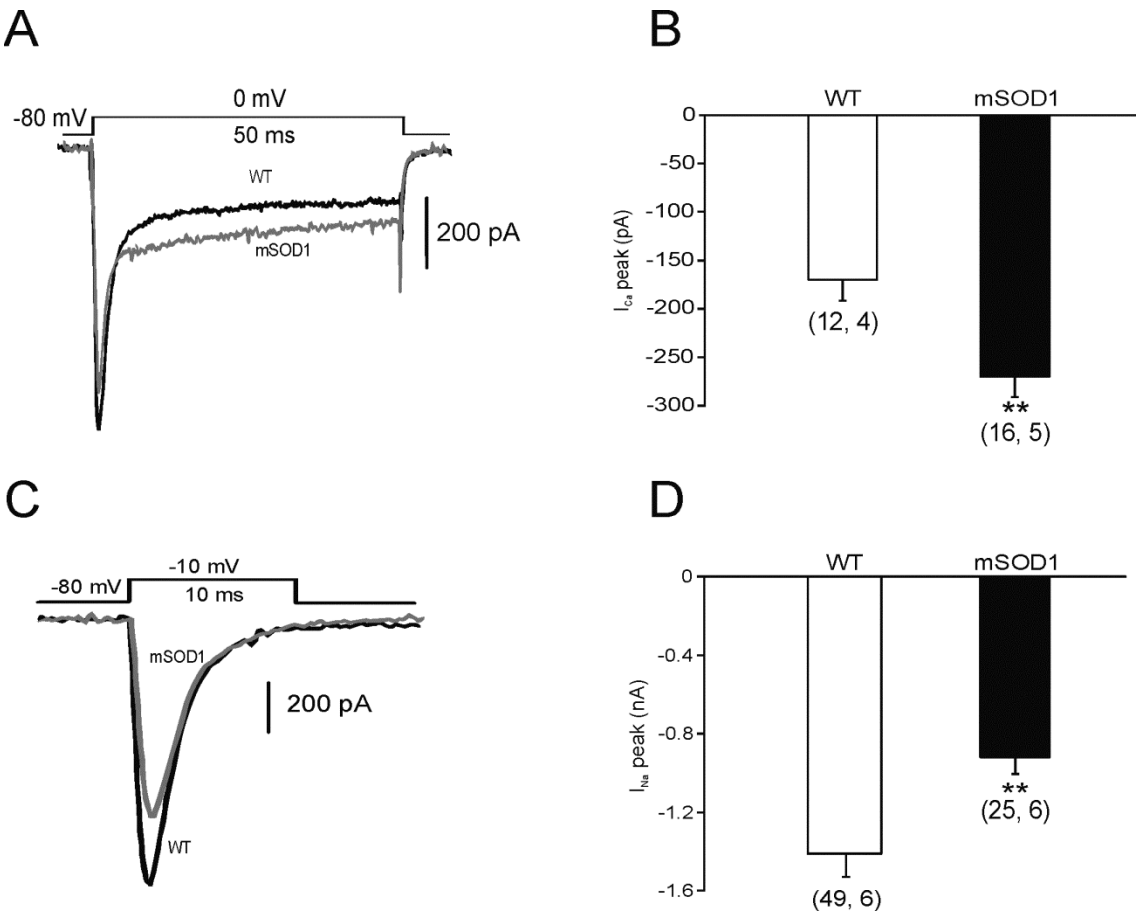
A
-80 mV
0 mV
50 ms
WT
mSOD1
200 pA
B
WT
mSOD1
0
-50
-100
-150
-200
-250
-300
I_{Ca} peak (pA)
(12, 4)
**
(16, 5)
C
-80 mV
-10 mV
10 ms
mSOD1
200 pA
WT
D
WT
mSOD1
0
-0.4
-0.8
-1.2
-1.6
I_{Na} peak (nA)
**
(25, 6)
(49, 6)

FIGURE 4.

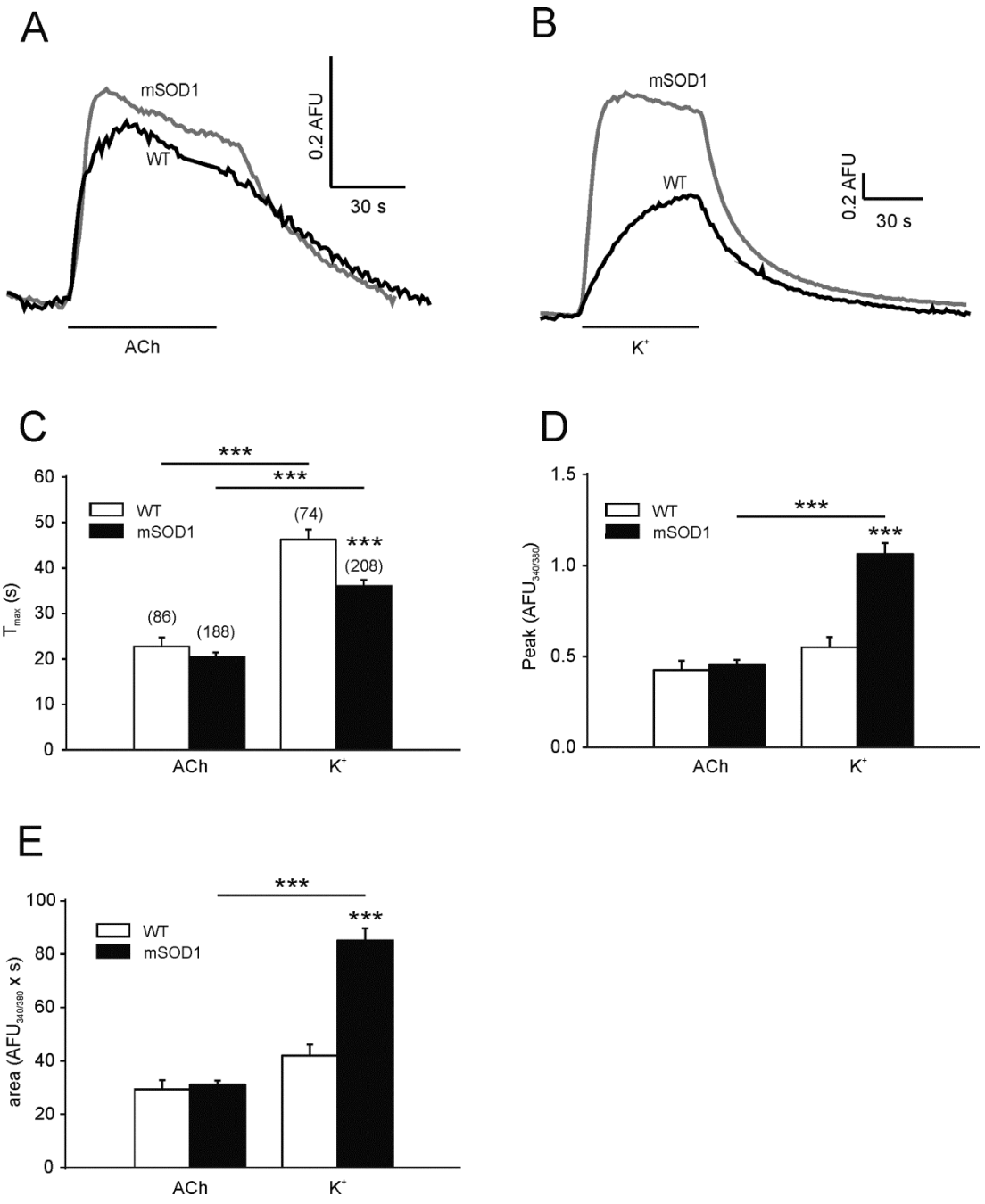
A
mSOD1
WT
0.2 AFU
30 s
ACh
B
mSOD1
WT
0.2 AFU
30 s
K+
C
***
***
WT
mSOD1
(74)
***
(208)
(86)
(188)
Tmax (s)
60
50
40
30
20
10
0
ACh
K+
D
***
***
WT
mSOD1
Peak (AFU340/380)
1.5
1.0
0.5
0.0
ACh
K+
E
***
***
WT
mSOD1
area (AFU340/380 x s)
100
80
60
40
20
0
ACh
K+

FIGURE 5.

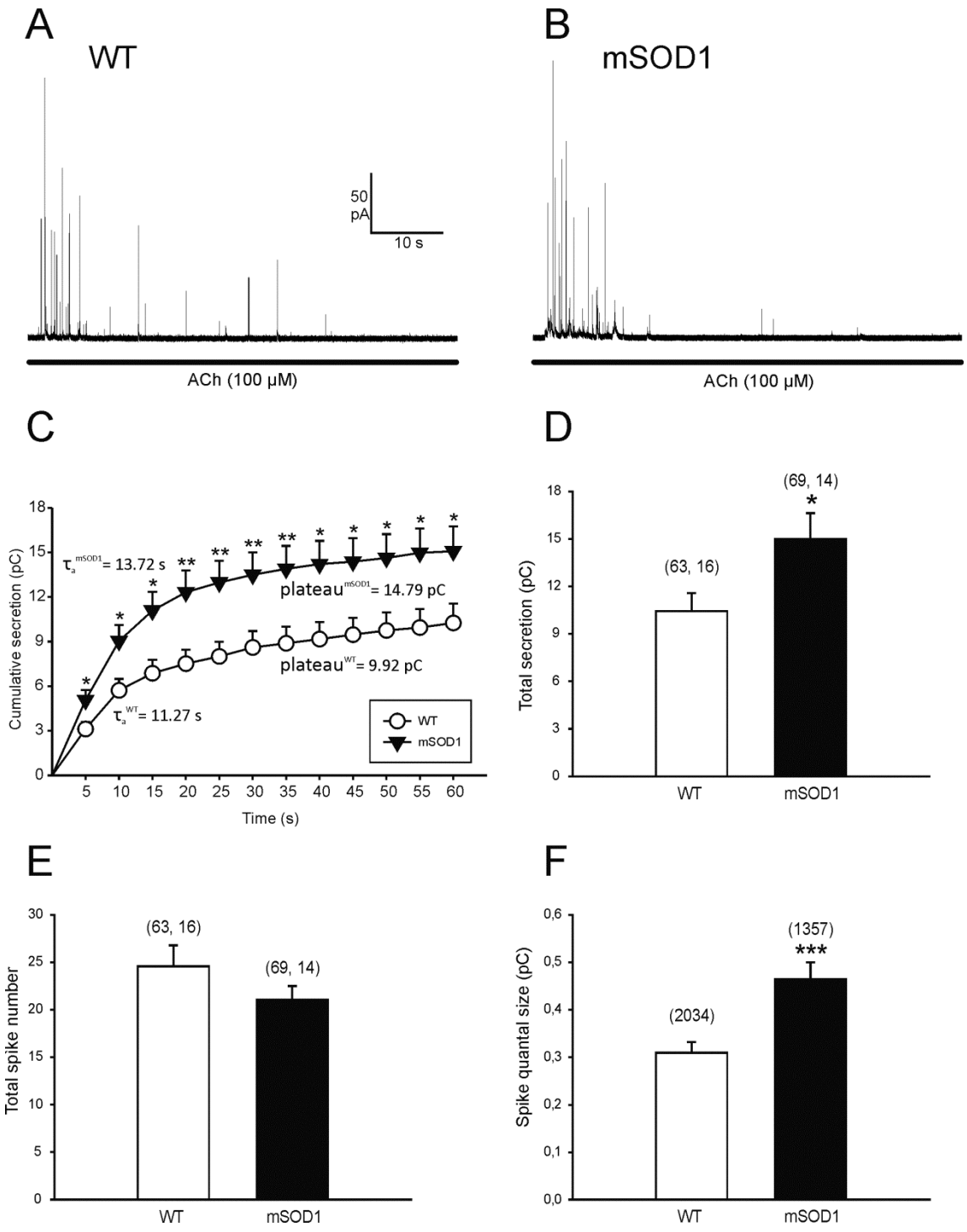
A
WT
50 pA
10 s
ACh (100 µM)
B
mSOD1
ACh (100 µM)
C
Cumulative secretion (pC)
Time (s)
τa mSOD1 = 13.72 s
plateau mSOD1 = 14.79 pC
plateau WT = 9.92 pC
τa WT = 11.27 s
WT
mSOD1
D
Total secretion (pC)
(63, 16)
(69, 14)
WT
mSOD1
E
Total spike number
(63, 16)
(69, 14)
WT
mSOD1
F
Spike quantal size (pC)
(2034)
(1357)
WT
mSOD1

FIGURE 6.

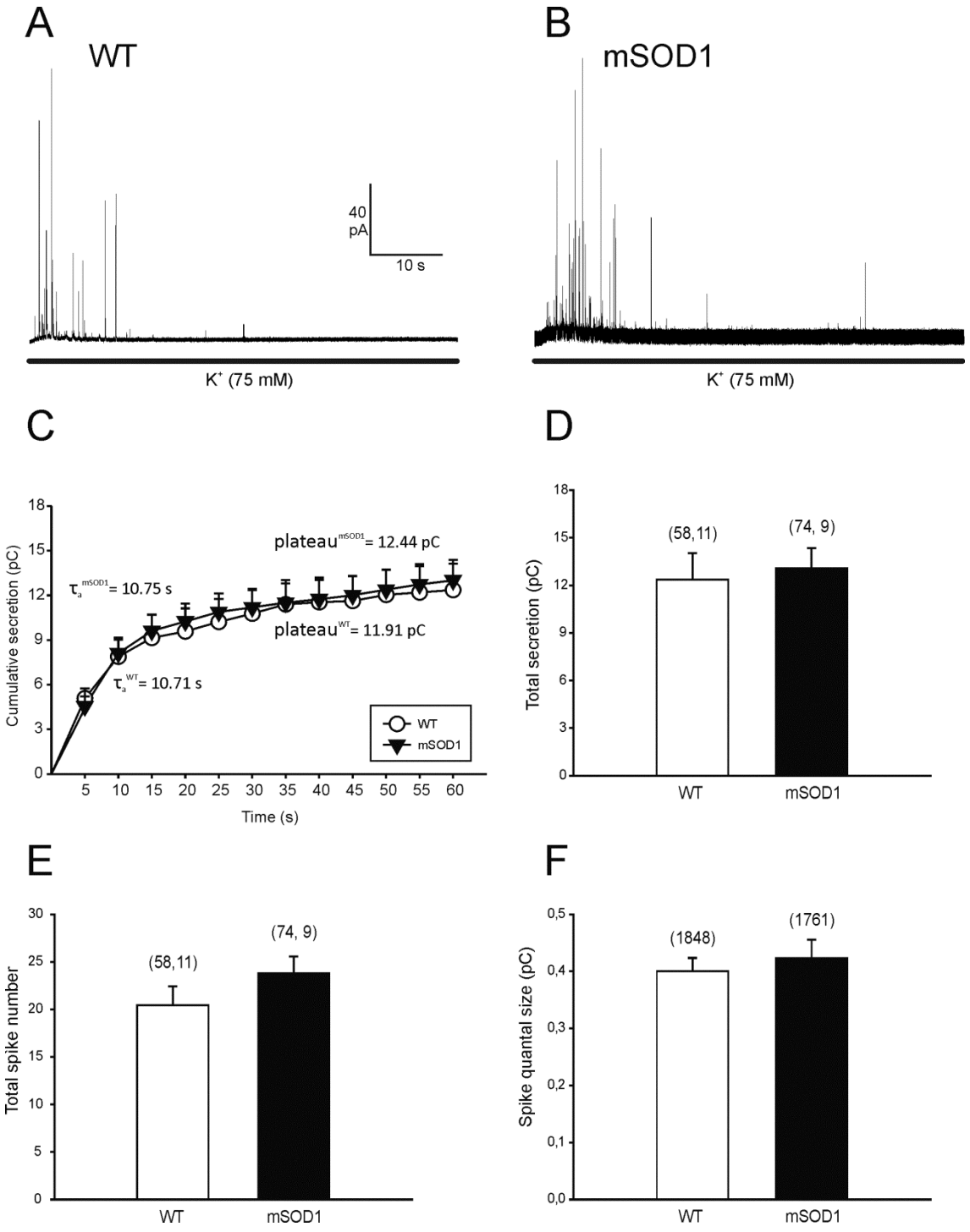
A
WT
40 pA
10 s
K+ (75 mM)
B
mSOD1
K+ (75 mM)
C
Cumulative secretion (pC)
plateau mSOD1 = 12.44 pC
τa mSOD1 = 10.75 s
plateau WT = 11.91 pC
τa WT = 10.71 s
WT
mSOD1
Time (s)
D
Total secretion (pC)
(58,11)
(74, 9)
WT
mSOD1
E
Total spike number
(58,11)
(74, 9)
WT
mSOD1
F
Spike quantal size (pC)
(1848)
(1761)
WT
mSOD1

FIGURE 7.

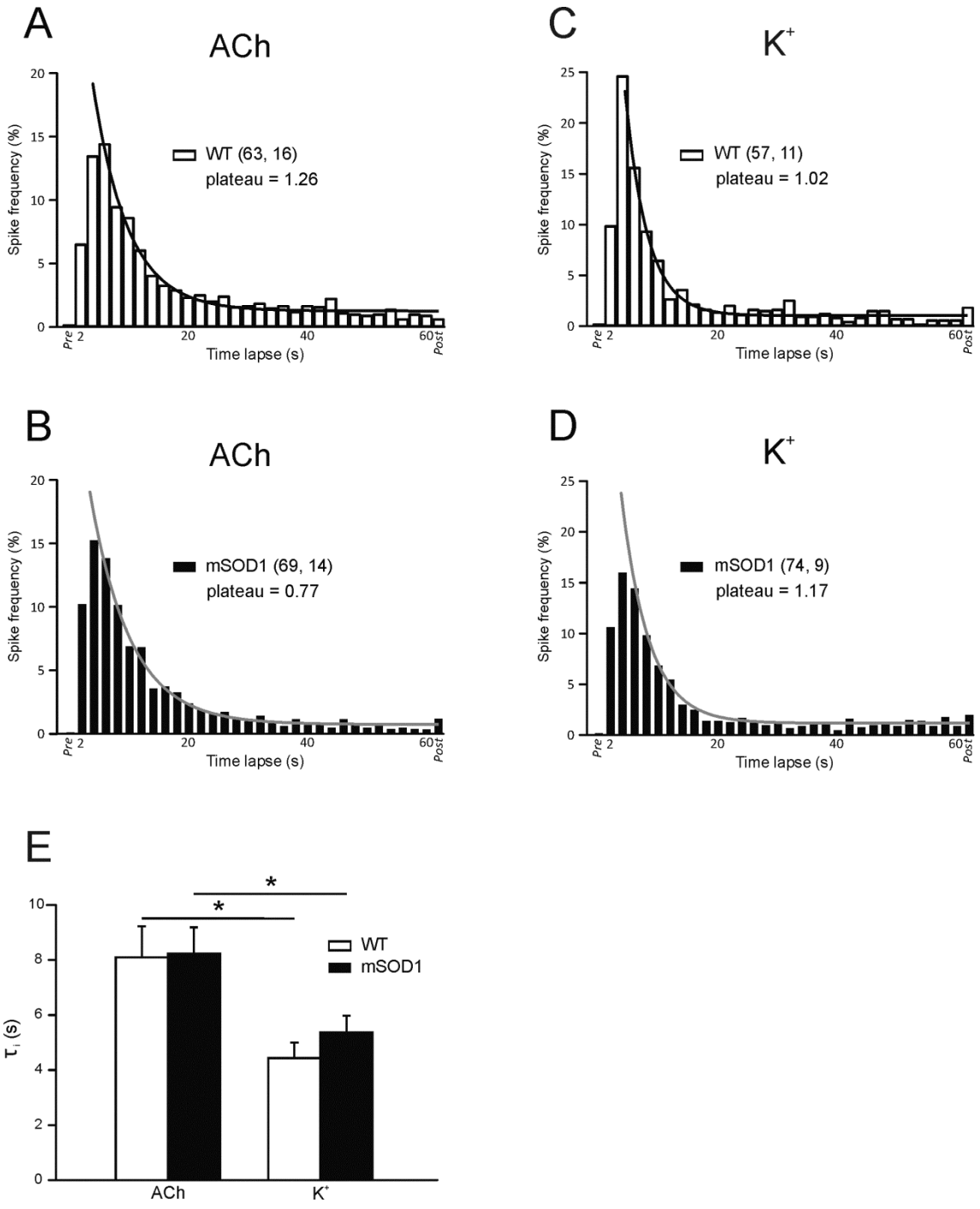
A
ACh
WT (63, 16)
plateau = 1.26
Spike frequency (%)
Time lapse (s)
Pre
Post
B
ACh
mSOD1 (69, 14)
plateau = 0.77
C
K+
WT (57, 11)
plateau = 1.02
D
K+
mSOD1 (74, 9)
plateau = 1.17
E
WT
mSOD1
τi (s)
ACh
K+
*
*

FIGURE 8.

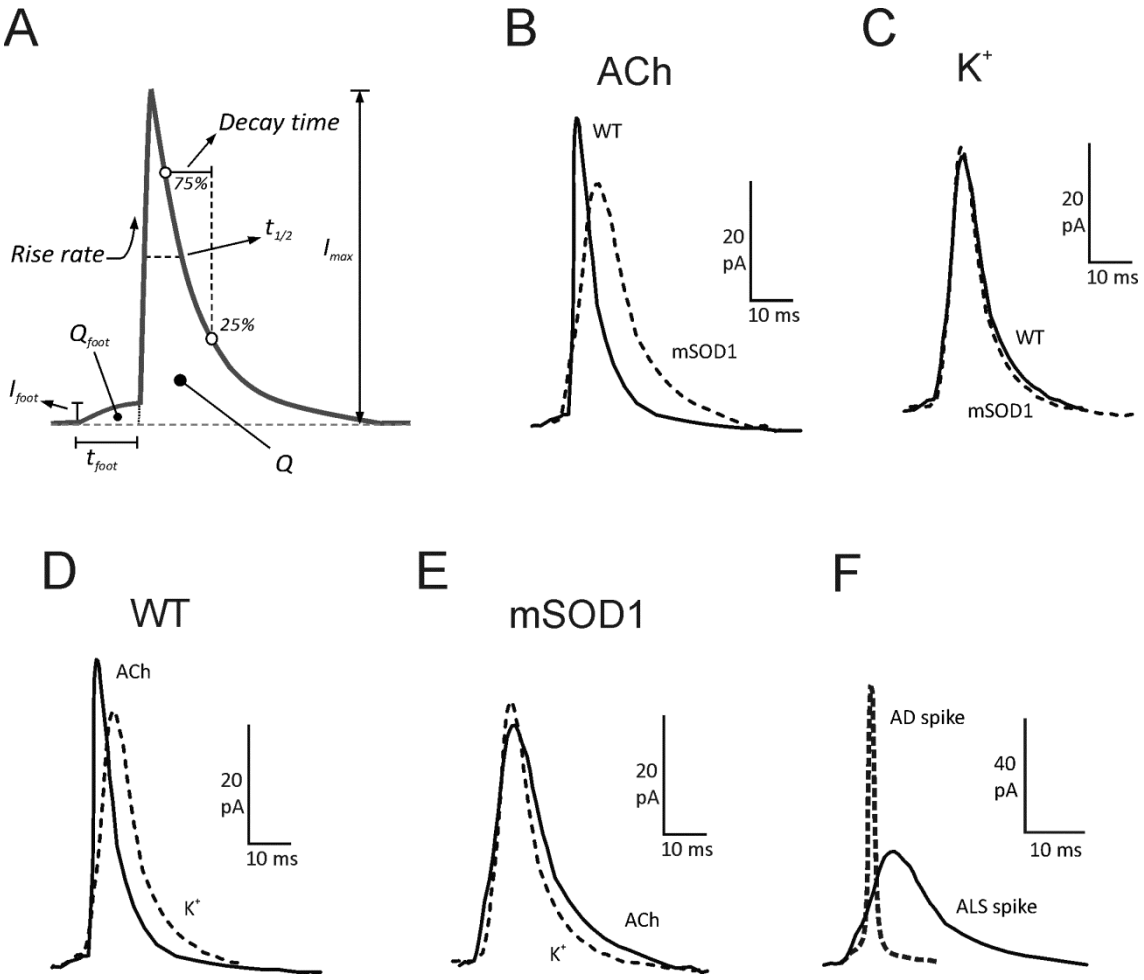
A
Decay time
75%
Rise rate
$t_{1/2}$
I_{max}
25%
Q_{foot}
I_{foot}
t_{foot}
Q
B
ACh
WT
20 pA
10 ms
mSOD1
C
K^+
20 pA
10 ms
WT
mSOD1
D
WT
ACh
20 pA
10 ms
K^+
E
mSOD1
20 pA
10 ms
ACh
K^+
F
AD spike
40 pA
10 ms
ALS spike

FIGURE 9.

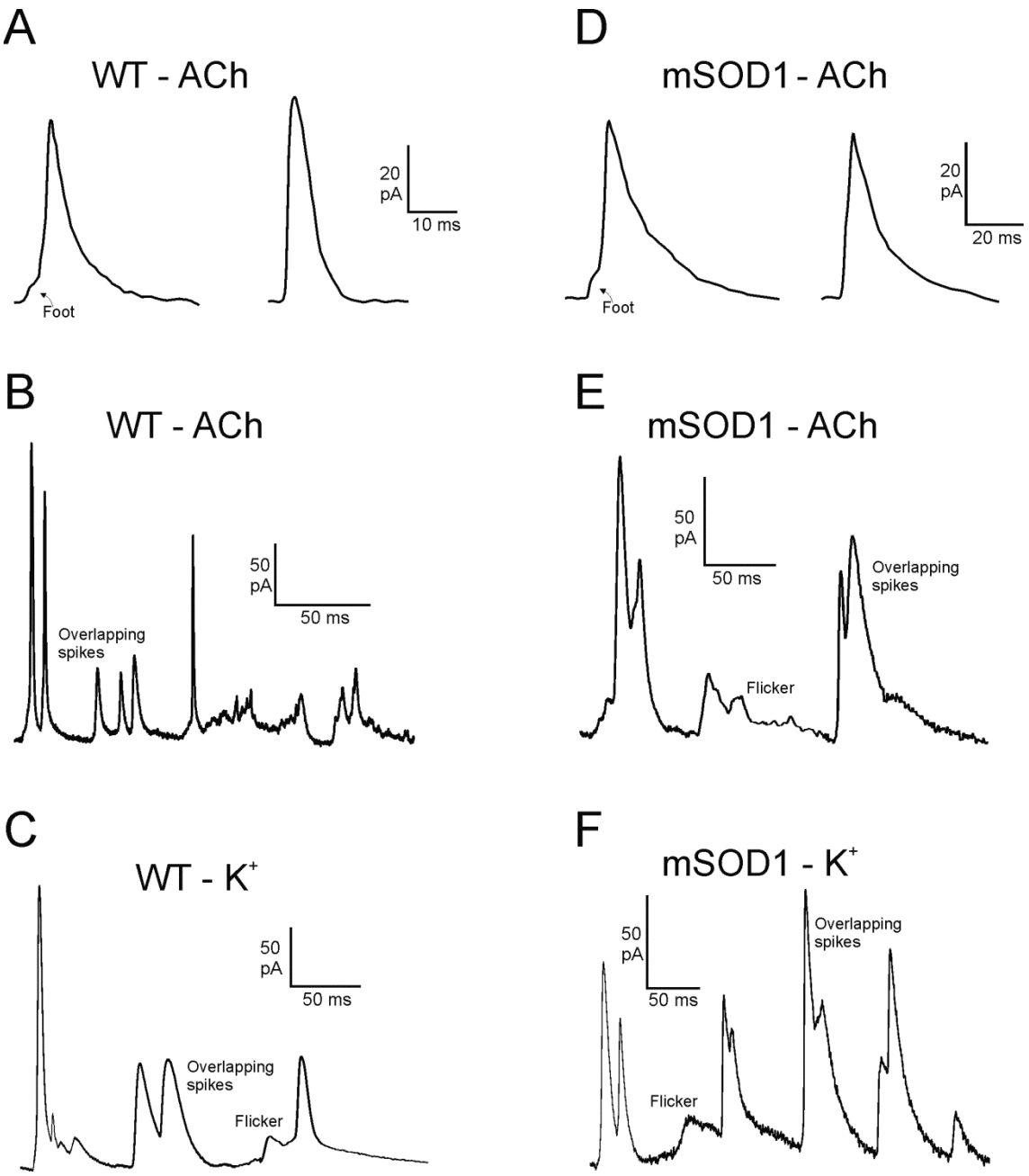
A
WT - ACh
20
pA
10 ms
Foot
D
mSOD1 - ACh
20
pA
20 ms
Foot
B
WT - ACh
50
pA
50 ms
Overlapping
spikes
E
mSOD1 - ACh
50
pA
50 ms
Overlapping
spikes
Flicker
C
WT - K+
50
pA
50 ms
Overlapping
spikes
Flicker
F
mSOD1 - K+
50
pA
50 ms
Overlapping
spikes
Flicker

FIGURE 10.

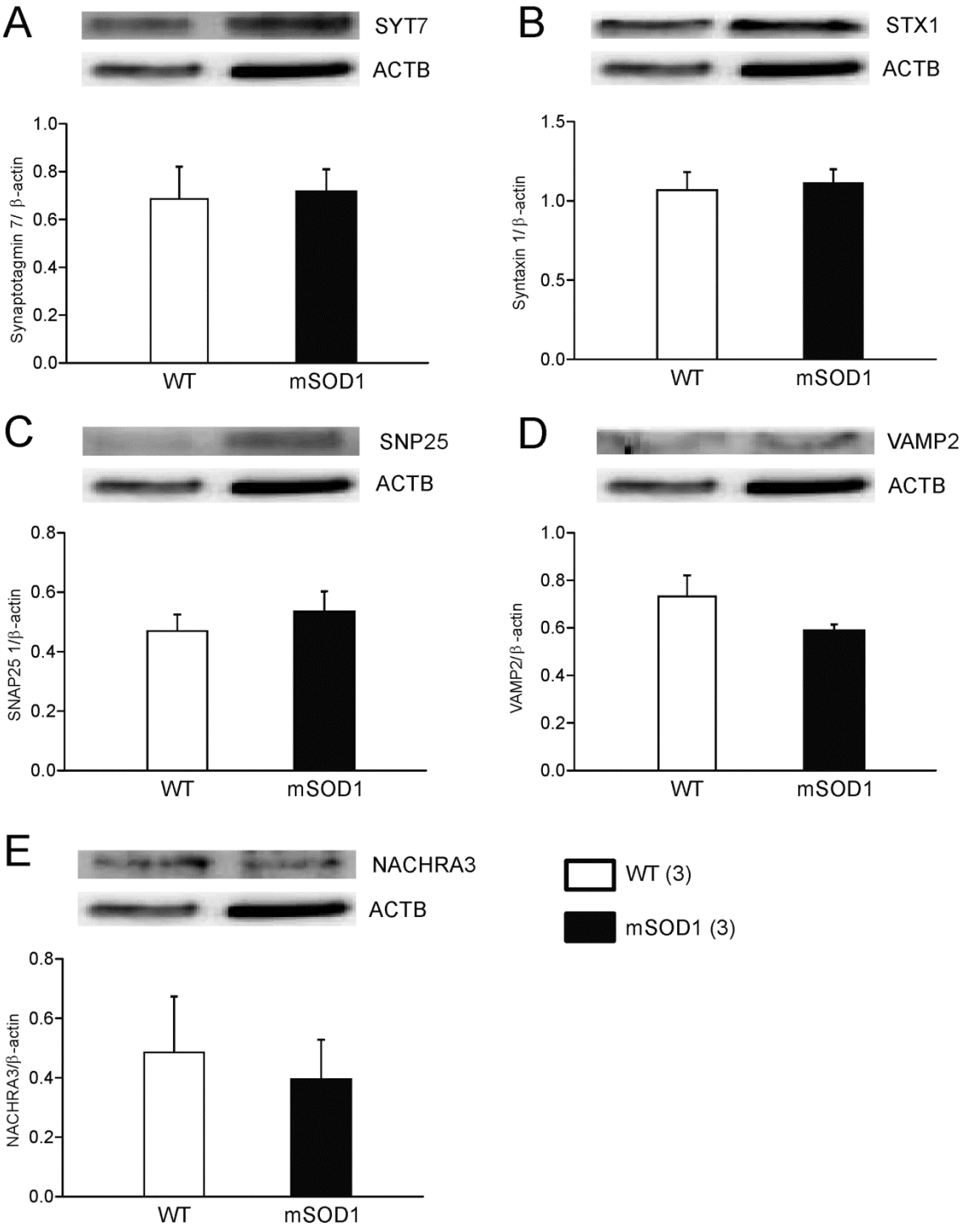
A
SYT7
ACTB
Synaptotagmin 7/ β-actin
1.0
0.8
0.6
0.4
0.2
0.0
WT
mSOD1
B
STX1
ACTB
Syntaxin 1/β-actin
1.5
1.0
0.5
0.0
WT
mSOD1
C
SNP25
ACTB
SNAP25 1/β-actin
0.8
0.6
0.4
0.2
0.0
WT
mSOD1
D
VAMP2
ACTB
VAMP2/β-actin
1.0
0.8
0.6
0.4
0.2
0.0
WT
mSOD1
E
NACHRA3
ACTB
NACHRA3/β-actin
0.8
0.6
0.4
0.2
0.0
WT
mSOD1
WT (3)
mSOD1 (3)

FIGURE 11.

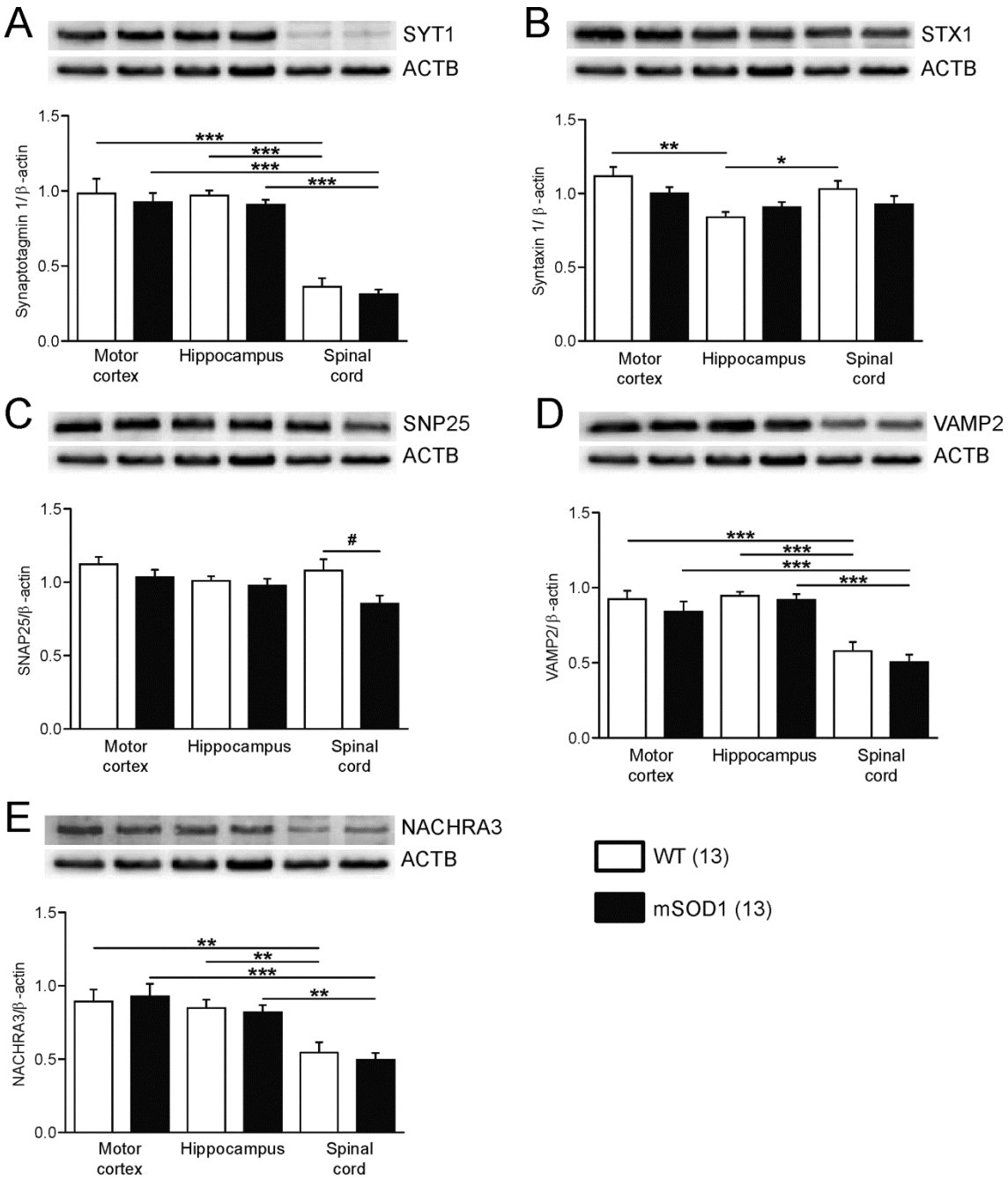
A
SYT1
ACTB
Synaptotagmin 1/β-actin
1.5
1.0
0.5
0.0
***
***
***
***
Motor cortex
Hippocampus
Spinal cord
B
STX1
ACTB
Syntaxin 1/ β-actin
**
*
C
SNP25
ACTB
SNAP25/β-actin
#
D
VAMP2
ACTB
VAMP2/β-actin
E
NACHRA3
ACTB
NACHRA3/β-actin
**
WT (13)
mSOD1 (13)

FIGURE 12.

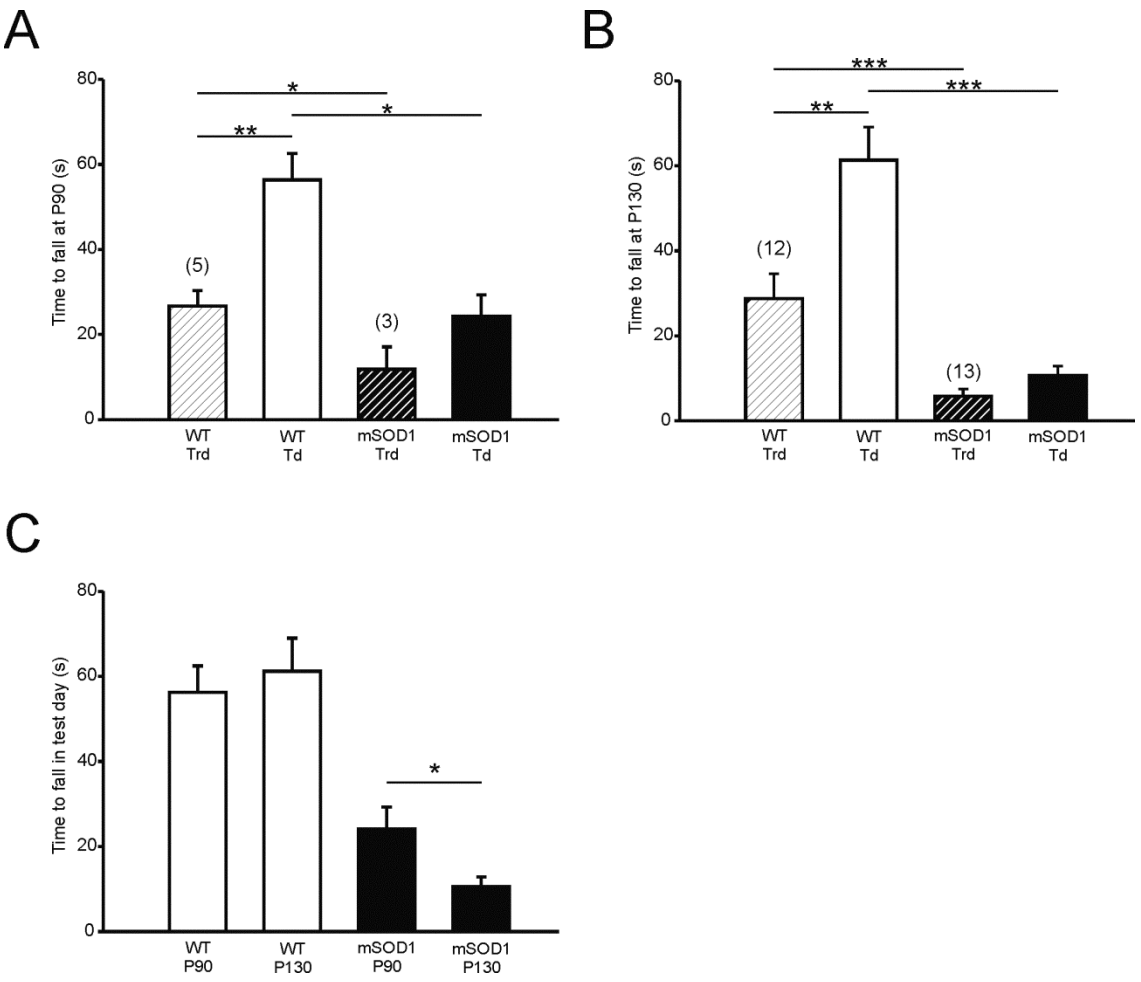
A
Time to fall at P90 (s)
80
60
40
20
0
*
*
**
(5)
(3)
WT Trd
WT Td
mSOD1 Trd
mSOD1 Td
B
Time to fall at P130 (s)
***
***
**
(12)
(13)
WT Trd
WT Td
mSOD1 Trd
mSOD1 Td
C
Time to fall in test day (s)
*
WT P90
WT P130
mSOD1 P90
mSOD1 P130

TABLES

TABLE 1.

Cell type (stimulus)	Events (cells)	Rise rate (pA/ms)	Decay 75-25% (ms)	$t_{1/2}$ (ms)	I_{max} (pA)	Q (pC)
WT (ACh)	2034 (63)	23.75 ± 2.49	6.06 ± 0.38	5.71 ± 0.32	39.25 ± 3.17	0.31 ± 0.02
mSOD1 (ACh)	1357 (69)	15.21 ± 1.15 ** (35.94% lower)	9.73 ± 0.6 *** (60.7% higher)	8.86 ± 0.56 *** (55.3% higher)	32.72 ± 2.08 * (16.62% lower)	0.47 ± 0.03 *** (52.24% higher)
WT (K^+)	1848 (58)	17.19 ± 1.38 # (27.62% lower)	7.69 ± 0.43 ## (27.05% higher)	6.94 ± 0.32 ## (21.57% higher)	34.16 ± 1.88 (12.97% lower)	0.4 ± 0.02 ### (28.77% higher)
mSOD1 (K^+)	1761 (74)	19.81 ± 1.31 ## (30.24% higher)	8.11 ± 0.55 # (16.43% lower)	7.28 ± 0.5 ## (17.81% lower)	36.69 ± 2.07 (12.12% higher)	0.42 ± 0.03 (10.2% lower)

TABLE 2.

Cell type (stimulus)	Events (cells)	Spikes with foot (%)	Multiple-spike events (%)	Flickering (%)
WT (ACh)	2034 (63)	59.56 ± 2.17	3.91 ± 0.46	6.9 ± 0.88
mSOD1 (ACh)	1357 (69)	65.71 ± 1.91 * (10.33% higher)	4.15 ± 0.55 (6.14% higher)	8.84 ± 0.94 (28.12% higher)
WT (K^+)	1848 (58)	67.94 ± 2.28 ## (14.08% higher)	5.69 ± 0.74 (45.52% higher)	7.52 ± 0.72 (8.99% higher)
mSOD1 (K^+)	1761 (74)	73.12 ± 1.72 ## (11.27% higher)	5.09 ± 0.57 (22.65% higher)	8.13 ± 0.91 (8.03% lower)

TABLE 3.

Cell type (stimulus)	Events (cells)	Spikes with foot (%)	t_{foot} (ms)	I_{foot} (pA)	Q_{foot} (fC)
WT (ACh)	2034 (63)	59.56 ± 2.17	3.6 ± 0.3	3.73 ± 0.22	17.08 ± 1.59
mSOD1 (ACh)	1357 (69)	65.71 ± 1.91 * (10.33% higher)	4.7 ± 0.26 *** (30.8% higher)	2.87 ± 0.14 *** (22.95% lower)	16.35 ± 1.13 (4.27% lower)
WT (K^+)	1848 (58)	67.94 ± 2.28 ## (14.08% higher)	4.14 ± 0.25 # (15.23% higher)	2.88 ± 0.23 ### (22.96% lower)	14.94 ± 1.3 (12.52% lower)
mSOD1 (K^+)	1761 (74)	73.12 ± 1.72 ## (11.27% higher)	4.19 ± 0.31 # (10.97% lower)	3 ± 0.14 (4.25% higher)	15.75 ± 1.49 (3.69% lower)